# 8
# Multiscale Study of Electrochemical Energy Systems

*Hany El-Sayed, Alois Knoll, and Ulrich Stimming*

## 8.1
## Introduction

The development of science has led to a huge diversification of approaches, methods and conclusions in investigating complex problems. While it is necessary to keep increasing the detail of the subjects being researched on, it becomes more difficult to fold the results back in an a priori, complex reality. It is not only the high degree of detail being covered that lets us forget where we originally started from but also the development of the different branches of science away from each other that makes it more difficult to combine results in a meaningful and scientifically correct way. Examples are the development between natural science on the one hand and, for example, engineering and medicine, on the other hand. The problems we are facing, for example, in the environmental and energy areas are so pressing that science solely as an intellectual playground cannot serve us for our future. Thus, recombining of what we have learned in the various disciplines is a necessity also for science to prove that it is useful for our future. Encouraging are approaches by theoreticians, for example, in natural science and engineering science, to attempt the so-called multiscale modeling that can bridge length scales from angstroms to meters. These attempts, however, show how difficult it is but understanding the necessity of such an approach is a crucial first step.

Electrochemistry started out mainly as an empirical and macroscopic branch of science until in the 1920s and 1930s when microscopic physical models were introduced due to Heisenberg's quantum theory. Today, electrochemical research is broadly positioned from theoretical and physical over analytical and biological electrochemistry to engineering and application. In this volume, two further aspects are covered: The history of electrochemical deposition processes in the electronics industry and, relevant also for the discussion in this chapter, the role of electrochemical engineering in battery research. In the broad spectrum of possibilities regarding the kind of approach to be taken, the question of identifying the important questions to be solved is rather controversial. A common perception is that the natural scientist solves molecular-based problems, then the

*Electrochemical Engineering Across Scales: From Molecules to Processes,* First Edition.
Edited by Richard C. Alkire, Phil N. Bartlett, and Jacek Lipkowski.

electrochemical engineer takes over the study of large-scale processes, and finally the mechanical engineer designs a device and brings it to functionality.

Such a process would be characterized as *bottom up*.

This serial process is tedious and time consuming and this may be part of the reason that even breakthrough discoveries at the level of natural science may take decades before they can be converted into technology and products are available on the market.

Another approach would try to use application and functionality as a starting point. Then, the various elements, for example, of a device, are described regarding their respective properties and functionalities. Improvements will be performed down to the molecular level. The efficiency of such an approach may be considerably higher since the functionality and performance are in focus from the very beginning. Typical design processes, such as the

- construction of fossil fuel power plants, wind and hydro power plants, solar thermal, photovoltaics,
- development of storage facilities, such as pressurized air, accumulator batteries, hydrogen, and solar fuels,
- construction of power grids, gas pipelines, hydrogen tanks,

are performed individually, and the resulting components optimized separately.

Such a process would be characterized as *top down*.

In comparing both approaches, the latter is more direct and is often quite successful. The former, however, may go through various sidelines; it is curiosity driven. This may be more of a zigzag course in terms of a specific application but bears the potential of being highly innovative in the end.

The conclusion is quite obvious; it is not good to have these two approaches as alternatives but rather in a combination. We need both qualities, and the question is how to organize this in a research environment. In the following is a schematic that tries to illustrate this (Figure 8.1).

In the three elements *systems*, *components,* and *fundamentals* top-down and bottom-up approaches should be pursued; in the systems section and the fundamentals section top-down and bottom-up, respectively, may be more important. In the end, the mixture of both is the decisive approach. "We need to develop a curiosity for what happens with my results, so I better understand what others do with my results." This helps to bridge the different sections.

In order to foster this kind of understanding, the purpose of this chapter is to attempt to draw a line in the example of an energy system that includes electrochemical processes from a system description and evaluation and the methods to analyze those to components, to materials and down to molecular functionality. This chapter is far from being comprehensive or even complete; it is rather sketchy but with the intention to show a continuous red line combining all levels of abstraction in such a complex system. So it should not be understood as the place where one can obtain the best description of the latest research results, but it has a conceptual character trying to point out how things belong together.

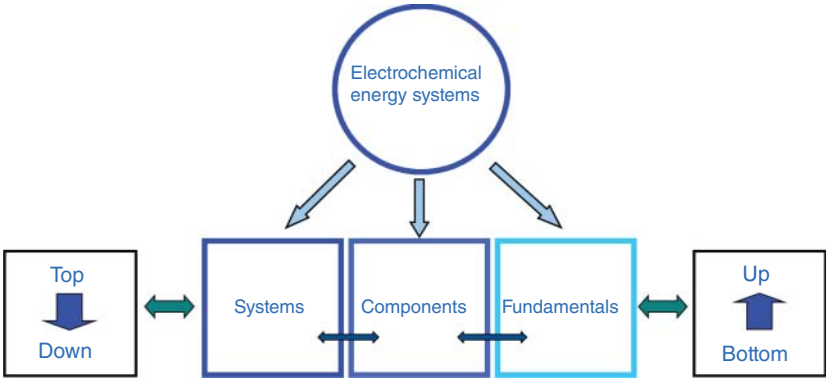


**Figure 8.1** Structure of an energy system with different components.

If this can be achieved, a better understanding of a complex research process is possible.

On the basis of the discussion above, the chapter is structured in a way that first the system and its boundary conditions are described and discussed. In this discussion also the question of organization and hierarchy is addressed from the point of computer science. Then, a very simple example is described as to how a building block in an urban city (example: Munich, Germany) is powered by renewables. It shows that more than three quarters of the annual electricity demand can be covered by renewables provided you have an appropriate energy storage and management. Further on, the case of an autonomous electricity supply is assumed based on renewables. A fuel cell system is conceived that is based on bioethanol obtained from biowaste. In this direct ethanol fuel cell (DEFC), the operational concept and the materials are discussed. In the end, the important aspect of electrocatalysis and its criteria for the DEFC are analyzed.

In the conclusions section, the results of the various sections are being put in perspective to each other. Especially, the aspect of *top down* versus *bottom up* is discussed again and compared to the principal ideas put up before. It is shown that the processes are not linear but rather circular in nature.

## 8.2
## Architectures of Energy Systems

As outlined above, energy technology is still strongly influenced by hardware developments, and it is essentially about the principles of energy conversion, energy storage, and energy transport. Until now, the meaningfully coupled design of these entities, as well as the organization of the practical operation of the resulting systems, has been dealt with only on a secondary level. One example is the ongoing discussion about “smart grids”: it is now generally understood that

computer science and communications engineering concepts will have to play a central role in both the planning and run-time phase of all layers of energy systems. This will become necessary, not only because the renewable energy supply typically fluctuates but also because there will be many more producers in close proximity to the electricity consumers, and with the advent and deployment of electric cars, storage capacity may not only be distributed, but may even be physically movable across large geographic *regions*.

### 8.2.1 The System and Its Boundary Conditions

Energy systems such as smart grids and their constituents (components and processes) are *systems of systems* [1]. The upcoming need for the holistic design, optimization, and operation of such systems at their various levels (from the molecule to the city) will give rise to a new interdisciplinary research field: *Computational Energy Science*.

There are two discernible phases in the lifetime of a smart multiscale and multisystem energy system:

1) *Design time:* based on a specification of system requirements, available components are considered to be candidate entities, and then and only then, can the subsystems be compiled. On the basis of simulations, the borders of the subsystems are defined and redefined in an iterative cycle such that the optimal functional units and cells emerge. These units will have to be implemented and connected via hardware; therefore, the result of this phase will be a static scheme. This will have to be done increasingly on computers with massive power, so that different scenarios can be investigated in detail, that is, "exploratory simulation."
2) *Run time:* when the system (composed of its subsystems) is in operation, the input, output, and dynamic requirements will change continuously depending on the timescale. To operate the system according to a set of optimality criteria, some kind of predictive simulation will be necessary. This simulation will make it possible to permanently adjust the internal system parameters to follow an optimal trajectory.

Both phases are based on suitable models of systems and component behavior. From an informatics perspective, a microgrid in a car will not be much different from a smart grid section formed by a small village because of the abstraction into computational models.

A typical future scenario is shown in Figure 8.2. The overarching smart grid can be *logically* divided into smaller cells (microgrids) that have a large autarky[1)]

1) There is frequently some confusion about the semantics of autonomy versus autarky. We understand *autarky* as the property of being self-sufficient and independent of external supply (e.g., a self-sufficient national economy that need not import raw materials from outside the country). By a*utonomy* we mean that an entity (creature, state, system) has the quality of being self-governed, that is, the rules according to which it functions can be changed on its own will.

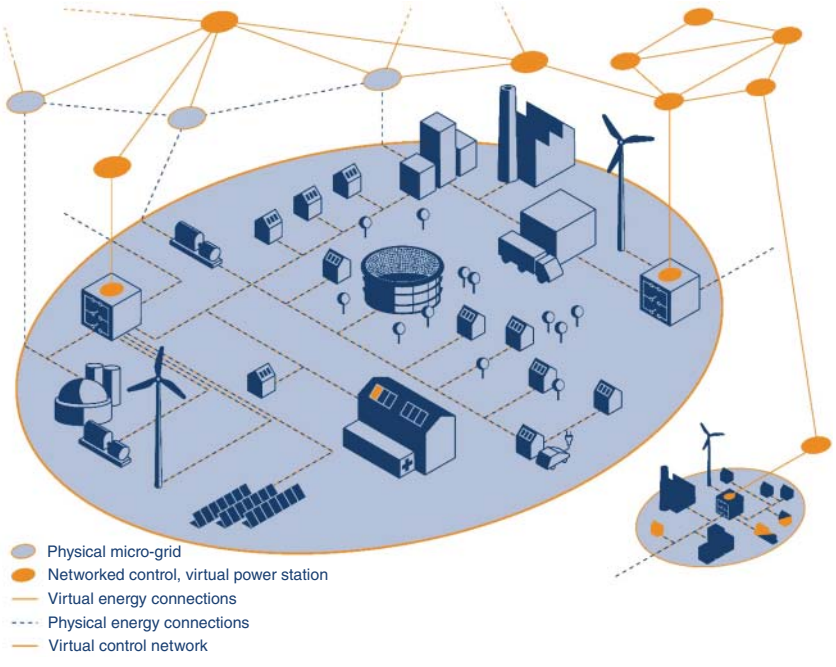


**Figure 8.2** Future scenario for smart grid and (physical) microgrids with virtual power stations. (Image adapted from Ref. [2]. Acatech, March 2012.)

of their own. The logical limits of the *virtual microgrid* do not necessarily correspond to spatial constraints (such as city limits or terrain topology) or to classical grid layers, such as voltage distribution levels. Nevertheless, by defining a border, both a real and virtual microgrid define a *region*; such regions are *autarkic* if there is no energy or material stream between them. Typically, they are *autonomous* if they can control the internal flows (energy and materials) inside their borders based on their own rules (and there is no entity outside their borders that has control over them).

This virtualization of the energy network has two consequences: (i) electricity production and consumption can be dynamically coupled and load production peaks can be compensated for very quickly, provided that the data exchange facilities between all of the entities of the network are powerful enough. (ii) For each component to be integrated into the management system, a corresponding data model is needed that can represent its (static) properties and (dynamic) behavior. The general goal is to *reduce energy exchange between regions to a minimum* so as to avoid transport losses and network fees.

This data-driven energy distribution management approach suggests that efficient management systems be developed first, from which the criteria for the design of concrete hardware and software systems can be derived. If the behavior model(s) of a complete grid at nano, micro, meso, and macro levels are defined

to the necessary degree of detail, realistic simulations of the energy flow can obviously be performed for an optimized planning of the grid (network topology, placement of storage elements, etc.).

However, if these models can also be computed at run time, a multivariate, multilevel, online optimization can be performed, in which all those parameters that cannot be measured (or are too costly to measure) can at least be estimated. The scientific question is then how the computational resources should be spread across the entire network and how they can use the communication pathways in the most efficient way, because a fine-grained simulation will have to cope with huge amounts of data (which should ideally be kept as local as possible, in full compatibility with the principles of local use and autarky).

Finally, it is important to realize that in the future, the flow in the network will not only become more fluctuant because more and more electricity from renewable sources will be fed into it – but also that the consumption will become more dynamic because electric transportation will play an increasingly more important role. Therefore, online planning based on real-time data is mandatory, and it may also prove to be very useful for integrating predictive simulations about other important aspects, such as the immediate future of the weather in a microgrid or short-term development of traffic and the resulting need for recharging electric vehicles. Consequently, energy science must deal with these questions, including the following:

- Development of *new architectural structures*, which interweave energy generation and consumer needs with distributed hierarchical layered "autonomy for autarky" concepts,
- Development of *behavior models of components* and models for these models (*meta-models*), as well as methods for creating these models in a straightforward manner,
- Definition and development of (Internet-based) *communication methods* for relaying status, planning, and scheduling information in real-time, with high accuracy and of the highest reliability and security to enable accurate monitoring and control of the network,
- Development of *mechanisms for decentralized*, *fault-tolerant control* with possible local and (semi-)automated balancing of production, storage, and consumption, including links to temporarily available energy buffers to maintain self-sufficiency.

### 8.2.2 Architectures of Multiscale Energy Systems

Energy systems are *networks* with a certain *topology* in which extraction, refinement, conversion, transportation, distribution, and utilization of different forms of energy take place to provide a set of services. An energy system involves multiple interconnected "energy chains" that provide a certain *energy service*. Inside one system, these energy chains may, to some extent, compete with each other as

there may be multiple possible chains that lead to the provision of the same energy service (e.g., having a constant flow of electricity in one's home – regardless of its origin, such as nuclear, fossil, solar). Clearly, today's energy systems are of an extremely high complexity, especially on a large scale with a huge amount of interconnected energy chains. Each of these individual chains contains a large number of components (technical subsystems), into which and out of which there are flows of material and energy (commodities). They are interconnected through transportation processes.

In order to make the properties of an energy system accessible to computer simulations and computer-assisted design, its overall structure (network topology and network components) and the relations between the components (commodity exchange processes) must be expressible in a machine-interpretable form.

The development of a formally describable model for such energy systems has happened over a long time, beginning in 1972 [3]. Based on this pioneering work, a Reference Energy System (RES) has been developed over the years [4]. The basic layout of an energy system is shown in Figure 8.3.

In [5], a new graphical representation and additional elements, which were not originally proposed by Hoffman [3], were introduced into the RES concept. They extend and enhance the original model by several concepts, which became necessary because of technology developments over time. In [6] and [7], these concepts were refined even further to become the extended RES (eRES) as available today. This is described in Figure 8.4.

Using this formal (and yet human-understandable) representation, we can attach clearly defined semantics to every energy system structure. In our context of multiscale energy systems, it is particularly important that energy systems are structured into *containers* (typically spatial regions), which can be part of a surrounding container. In other words, due to the concept of a recursively defined container, an arbitrary level of detail can be clearly specified in terms of "is part of" or "contains" relationships. There are just a few more terms that need to be defined here to provide a basic understanding:

- *A container* is the basic entity for constructing hierarchical structures among the elements of an eRES. Containers can be aggregated by "grouping" elements and, conversely, they can also be disaggregated. Depending on the (variable) definition of their semantics, containers can be seen as regions for a geographical separation, or as a specific technology, for example, containing all elements consuming fossil fuel, and so on.
- *A process* is a representation of an arbitrary physical device, which transforms commodities into other commodities. For practical usage, they have to be further specialized into internal or exchange processes.
- A *commodity* is defined as a material stream or a set of streams that are quantitatively ascertainable and that are produced and consumed by other processes. They are typically even further categorized as internal, input, and output commodities. Storage as such is also introduced as a commodity that can be exchanged for another commodity (e.g., a fuel) for different periods of time, while the act of storing is seen a process.

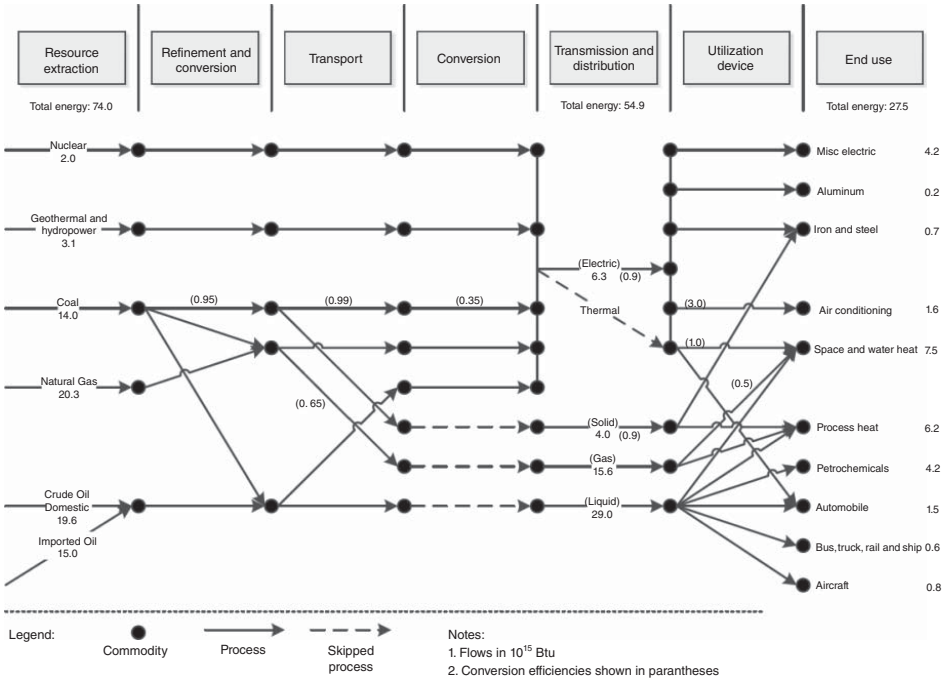


**Figure 8.3** Example of an energy system in formal graphical notation showing the relationships between all of the defining elements of an RES using the original graphical RES representation. (Adapted from Ref. [4].)

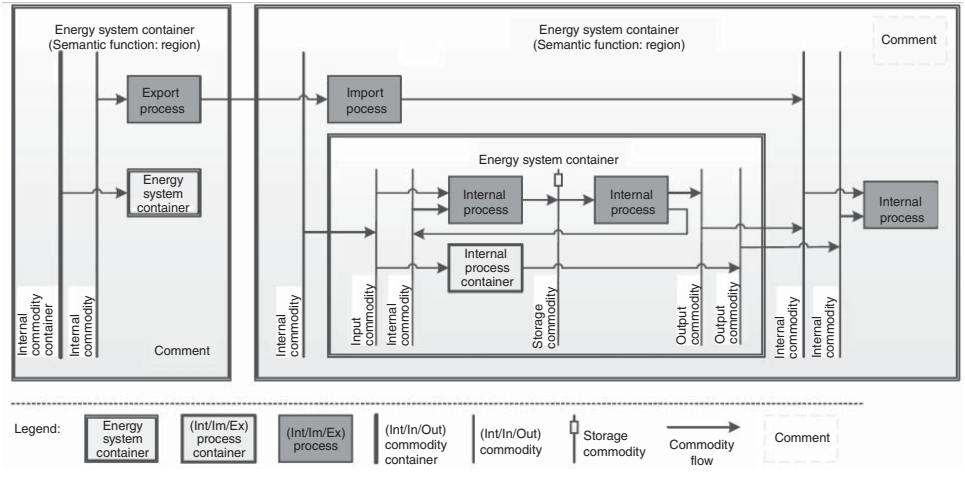


**Figure 8.4** Abstract energy system showing the relationships between all of the defining elements of an eRES using the graphical eRES representation.

Notably, the concept of containers makes it possible to create top-down as well as bottom-up models in the eRES notation. In a bottom-up procedure, the elements are aggregated complex energy systems. In the top-down "design mode," containers can be introduced that can later be gradually refined. Hence, the eRES notation is very ergonomic and user friendly, because the combined bottom-up and top-down approaches allow for hybrid modeling and extensions at any later point in time.

As part of our ongoing work, the conceptual definition of eRES has been transformed into a formal alternative language, the *Universal Scheme for modeling Energy Systems* (USES). The advantage of USES over eRES lies in its clearly defined concepts and their relationships with each other. USES is minimal in terms of its concepts, which means that no unnecessary exceptions are introduced. This represents a significant simplification compared to eRES while offering the same expressive power – and the same power for graphical representation as depicted above. A complete formal description of the syntax of USES that takes advantage of both graph theory and the unified modeling language (UML) class diagram language can be found in [8].

To illustrate the power of the approach, we can examine the network in Figure 8.2 in more detail. Figure 8.5 shows the same network, but with labeled entities: power stations; virtual power stations; PMG, physical microgrid; VPS,virtual power station; C, consumer; PP, power station; T, transformer. This network transforms into the graphical representation shown in Figure 8.6, employing the USES graphical language. This picture corresponds 1 : 1 to a formal textual description that can be read and processed by a computer.

This picture shows only the physical and virtual microgrids, whereas Figures 8.7 and 8.8 break down the physical microgrids PMG4 and PMG5 with their interconnected entities of real entities, such as power stations of various types, transformers, and individual consumers (houses, e-cars-charging stations).

While the formal representations of the imaginary smart grid in Figure 8.2 can be used to model a rather small grid with few components, the USES formalism is powerful and scalable enough to be utilized for the complete description and modeling of very large grids.

As an example, we can briefly review the electric power system of Singapore. Singapore can serve as an ideal example because (i) it is a small island with no connections to the outside world, (ii) the number of components is tractable even on small computers, (iii) the modeling of the entire network including its components can be completed in a short time frame, and (iv) the simulation can be performed in real-time to a great level of detail. Figure 8.9 shows the top-level topology of Singapore's electric energy system. There are a number of power stations that are connected to each other, there are smaller substations, and there are a number of components (switches, transformer stations, etc.) that need to be controlled in an adequate manner for the smooth general operation of the grid.

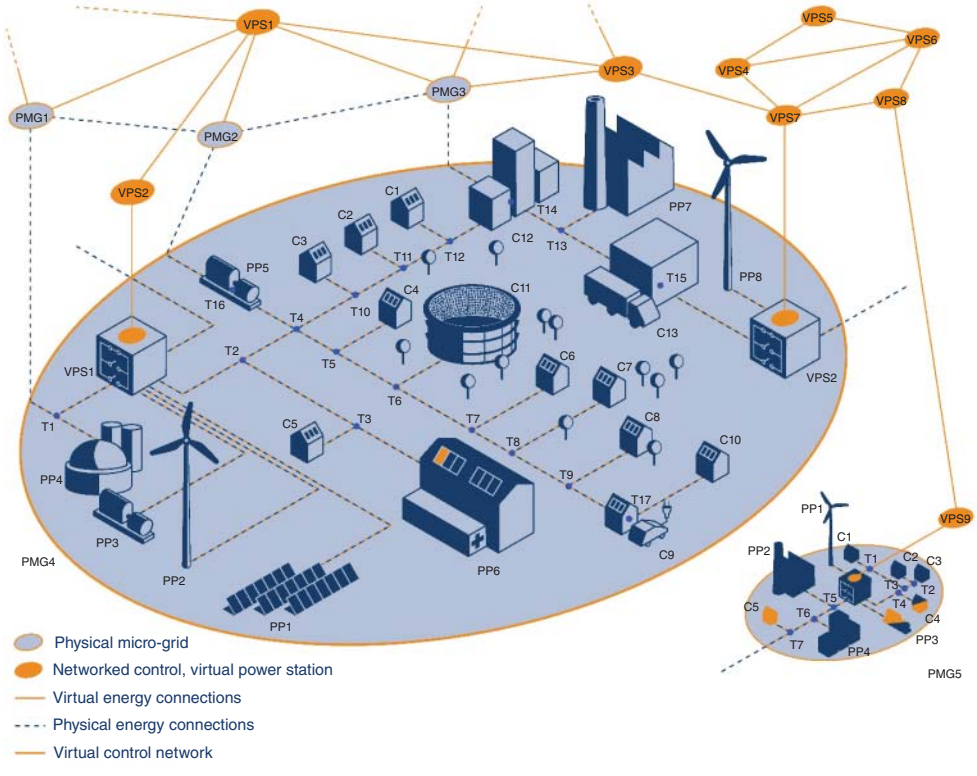


**Figure 8.5** Smart grid from Figure 8.2 with annotated entities. PMG, physical microgrid; VPS, virtual power station; C, consumer; PP, power station; T, transformer. (Image adapted from Ref. [2]. Acatech, March 2012.)

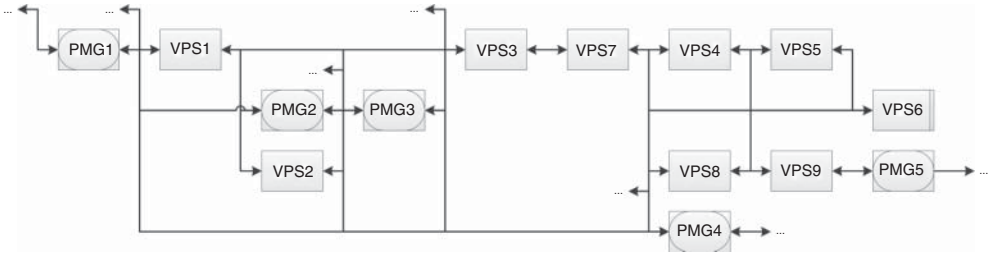


**Figure 8.6** Representation of labeled smart grid from Figure 8.2 with annotated entities.

In order to present a basic impression of what this system would look like in graphical USES notation, we transformed the topology (together with some additional knowledge of the stations and the grid) into a logical description of the grid (see Figure 8.10).

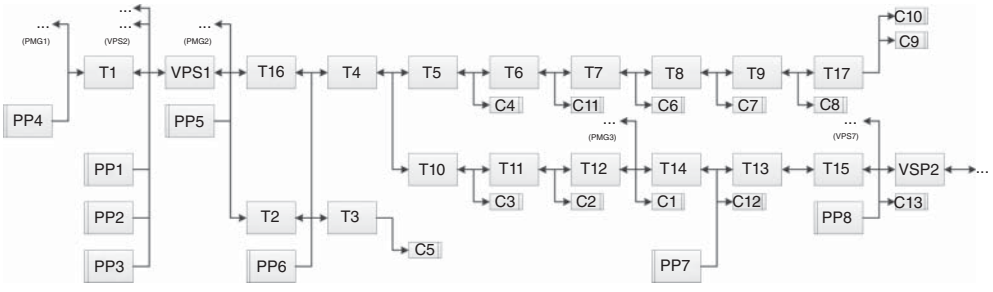


**Figure 8.7** Disaggregated PMG4. This physical microgrid breaks down into a number of power stations, transformers, and consumers.

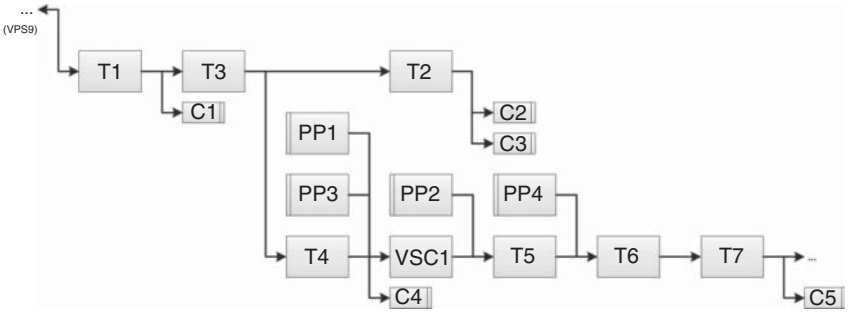


**Figure 8.8** Disaggregated PMG 5. Breakdown of the "small" physical microgrid in Figure 8.2 with its associated consumers.

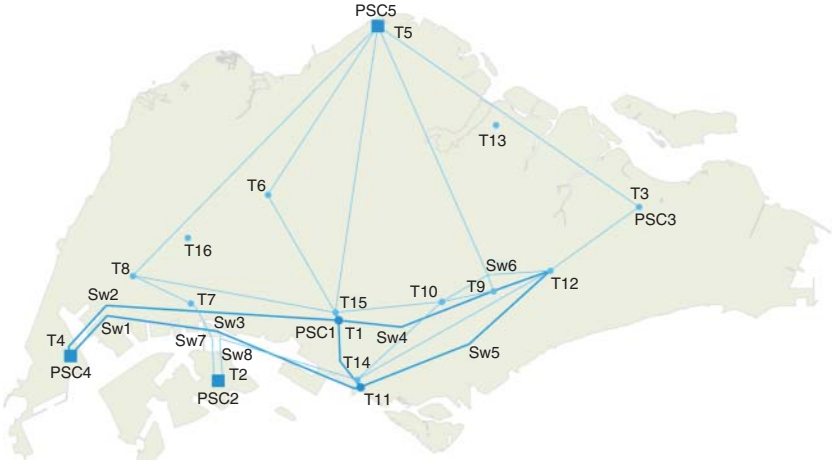


**Figure 8.9** Outline of the power conversion and transmission system of Singapore. There are five power station compounds PSC1–PSC5, each consisting of a number of power stations. There are also switches Sw1–Sw8 and transformer stations T1–T16; not all of them are shown in this picture.

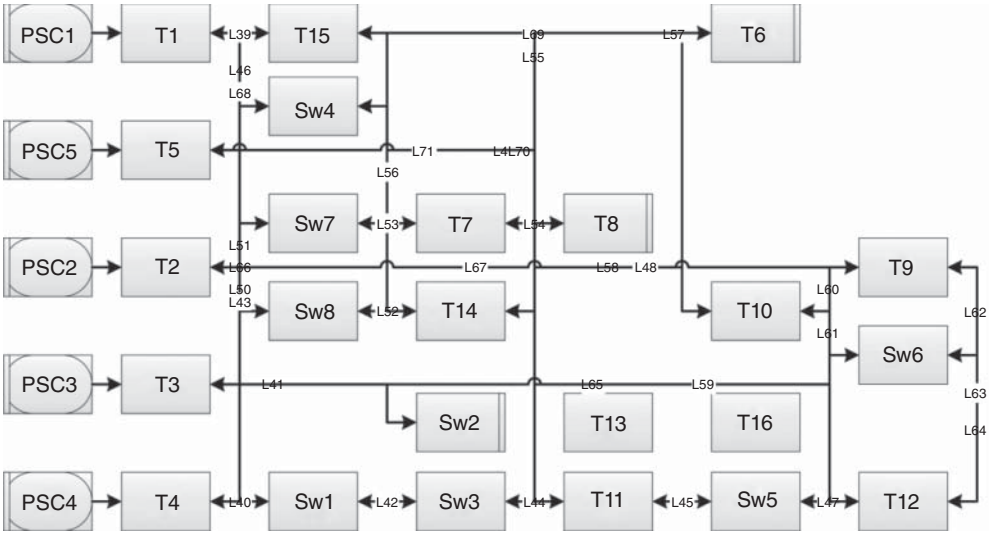


**Figure 8.10** Model of the power system in Singapore in USES graphical notation, with power lines shown as commodities. The boxes represent each entity of the grid; each box can be broken down into a more fine-grained, lower level description. This model can be used directly for all modeling purposes (at design time and at run time).

Figure 8.10 shows the five power station compounds (PSC1 to PSC5) as aggregated source processes (where each one contains a number of power stations on a lower hierarchical level, which is not shown in the picture). PSC1 to PSC5 are connected to transformers (T1 to T13) that distribute the energy via power lines (commodities L40 to L70), isolated transformers (T13, T16), and switches (Sw1 to Sw8) to the consumers. All of the modeled entities combined constitute the power transmission system of Singapore.

As mentioned before, this is only a very rough overview of the power of the USES approach. It is important to keep in mind, however, that it is the first approach to modeling complete systems in a consistent and uniform way – from the top level power stations down to the smallest consumer – so that these systems become computationally tractable – both at design time and later at run time (with the potential to transform the necessary models automatically between these two phases). In particular, the run-time models of component behavior are an essential element for the run-time optimization approach outlined in the following subsection.

### 8.2.3 Agent-Based Approaches for Run-Time Simulation and Optimization

Until now, we have only considered the energy flow in the heterarchy (or hierarchy) of systems. We tacitly assumed that the control of this flow would follow some basic rules; typically, in real systems the control is static (i.e., determined

at design-time) or moderately dynamic, in that it follows some time and demand profiles over a day, a week, or a year.

In future virtual autonomous networks, however, each component of the systems is connected to the overlaying data network – resulting in complete communication "reachability" between all devices. This means that all the network components can control their behavior according to knowledge about the state of the complete system, that is, they are permanently informed about the needs (of consumers), the supply situation (of power stations), the overall strategy to be followed (as determined by the network operator) as well as additional system-related information, such as failure or overload of components.

This gives rise to the question of how such a network can be efficiently organized according to a super-ordinated general goal (expressed by a target function). This goal could be the overall minimization of transport losses, the optimal scheduling of device operation, the management of supply in certain places, or any combination of these. The control strategy must be scalable (the number of devices in the network will increase over time), it must be robust (there will always be communication and/or component failures), and it must be adaptive (the operational requirements will change at various timescales). Furthermore, the strategy must be implementable on the most diverse computer platforms and embedded systems, it must be straightforward to realize, and it must enable the components to phase into and out of the complete network at any time ("plug-and-play"). Such a system would be characterized by the following key properties:

- *Simplicity:* the interfaces between the power system components (hardware and software) should be easy to implement and the components' operation should be transparent, that is, easy to monitor.
- *Fault tolerance:* If an individual component is detected as being temporarily or permanently defective, it should be automatically phased out of the normal system operation and, if possible, replaced with one or more alternative components. The system's performance should always degrade gracefully; it should never come to a complete stop.
- *Self-organization:* the distributed power system must be able to form "teams" of cooperating components (agents) in (virtual) cells. At run time, team formation must be completely automatic, that is, only dependent on the tasks to be performed (and on the state of the environment).
- *Heterogeneity and integration:* the system should allow for the transparent combination of components of different principles of operation and of different performance levels. It must be possible to establish online control loops on demand, which makes it necessary to provide communication modes that guarantee real-time interaction between all individual components.

As outlined in [8] for sensor networks, our approach to solving this multifaceted problem space is the *contract network protocol* [9, 10]. The extension to power systems (which are, in essence, sensor-actuator-networks) is straightforward. Before doing so, let us briefly look at *organization theory* [11], which forms the basis for our study.

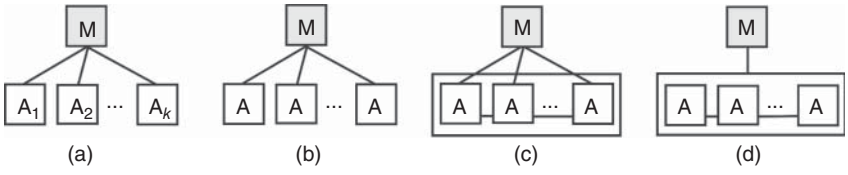


**Figure 8.11** (a–d) Different forms of hierarchical organizations.

The "nucleus" – the smallest functional unit – of our overall model of power system organization is an *agent*, that is, a network component with some functionality (conversion, distribution, storage), together with an automatic controller and some communication abilities. The agent is connected to the network. It can control its own behavior over an infinite period of time, but it can also correspond with any other agent in the network to synchronize its behavior with other agents. Synchronized agents are called *teams*, and teams can form over time – in a transient or a permanent manner. The *team structure* is specified by the relations between team members. These depend on the capabilities of the team members, which are defined by assigning competences and responsibilities to them.

An obvious choice for a structure is the simple hierarchy in Figure 8.11a, where the agents $A_1 \ldots A_k$ at the lower level all specialize in unique classes of tasks (for which they are individually competent and take responsibility). In an example from human organizations, the mandator M would be an executive officer who wants a report to be printed and bound and who controls every step in this process by successively having it typed ($A_1$), copied ($A_2$), and so on.

In the context of our smart grid, this implies that certain agents may specialize in particular tasks, such as power conversion; others work on different problems (e.g., bi-directional switching, up-down transformation, establishing communication paths, or coordinating subordinated agents). There need not be a temporal relation between agent operations (i.e., a certain operation is done before the other), but clearly a relationship between them in that they may all be sensibly coordinated by one superior mandator.

A different form of hierarchy is shown in Figure 8.11b, where a team of nonspecialized agents works on and returns complete solutions to the upper-level agent (e.g., a pool of typists are given tasks by the upper-level agent according to their current workload). This would correspond to several instantiations of the same agent type (with equal competences and duties) that can handle tasks depending on their current load – for example, an array of solar generators that can be individually controlled.

In an extended hierarchy there may be more than one level of coordinating agents. Agents at the lower level may communicate with each other (e.g., for computation load compensation), but they are still individually identifiable by the upper-level agents; see Figure 8.11c.

However, if there are nonspecialized agents on the same level, then there is a potential for these agents to coordinate themselves by exchanging information directly without any arbitration by a superior agent, Figure 8.11d. This is the

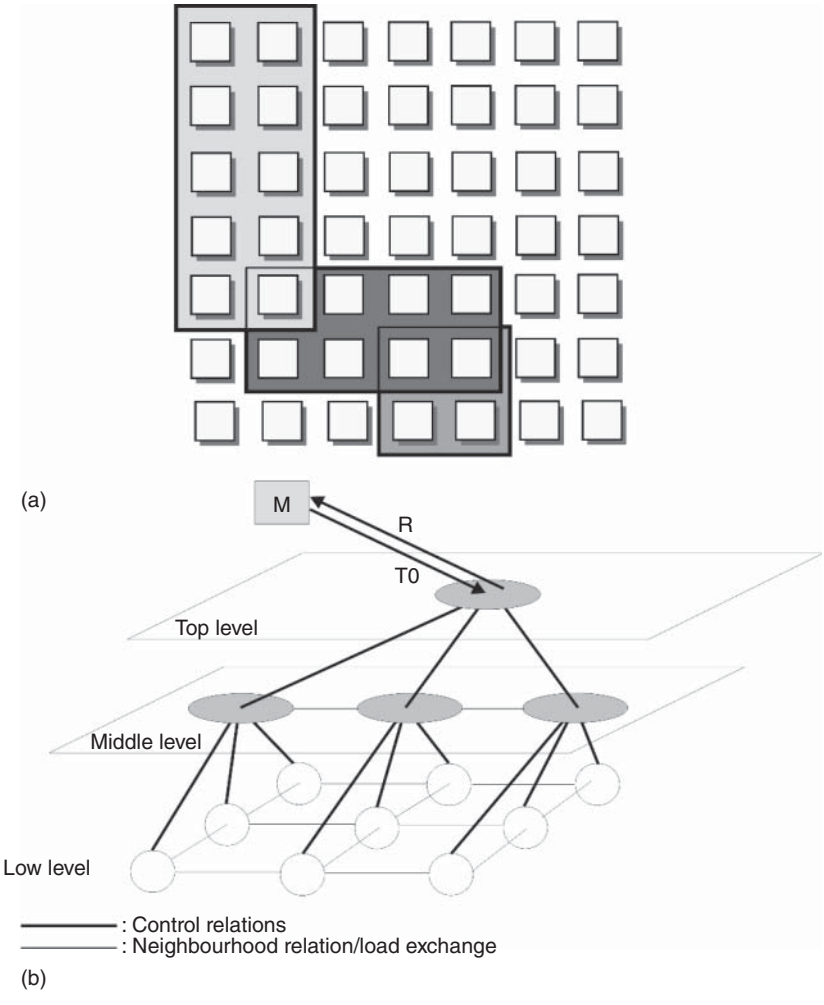


**Figure 8.12** The two basic structures – completely flat (a) and extended hierarchical (b).

concept of lateral structures. Both hierarchical and lateral structures may coexist in one network; subtrees are structured laterally and organize their cooperation within their layer of the subtree autonomously after receiving a certain task from their superior agent (or the external mandator M). In such organizations, there is no coordinating authority, and agents may be members of different transient teams.

In more detail, Figure 8.12a shows the situation for a completely flat organization: every agent can be a member of any team; teams are formed in a transient manner upon demand. The organization is completely determined by the task injected into the system and the current load, as well as system parameters. The shaded areas show different teams that may coexist (and may never appear in this

exact configuration again). Agents may be members of different teams at the same time (and have an internal queue for scheduling the activities they have to perform for the different teams). In an extended hierarchy (Figure 8.12b), there are flat structures at different layers. Layers on top of another layer can exert a certain level of control, that is, they manage the agent sets on the lower level and are managed by their upper level. While this concentration of decision power introduces single points of failure (there is only one top level agent), it also reduces the need for synchronization work, that is, bandwidth and time needed for forming a team.

As depicted below, usually no recommendation for structuring the network can be given a priori. Typically, only extensive simulations can answer this question. Clearly, however, given the power of today's networks, even this structuring can be dynamic – depending, for example, on the prevalent task at a certain time of the day.

Let us construct an example and assume that mandator M wants a certain task to be worked on, for example, the overnight recharging of a small number of electric cars in a neighborhood in the PMG. It injects this task into the network by negotiating with a number of candidate agents, and the first agent (called 1 in Figure 8.13a), which has the competence to communicate with the energy exchange broker, starts working on the task. It determines what the current price would be for importing electricity for recharging the car fleet – either simultaneously (all cars together) or sequentially (car by car over a longer period of time). It then hands over to agent 2 (again, after a negotiation phase with similar agents such as 2), which gathers local information from other agents about the state of the components (storage levels, current energy supply from power stations, expected consumption for the next few hours, etc.). Based on the information gathered, it constructs a plan for this specific situation. The execution of this plan is negotiated with other agents, which offer their services to agent 3 and have the ability to dispatch the recharging process (because they are part of the recharging infrastructure). In cooperation with agent 4, agent 3 then executes the charging; after its completion, billing and termination activities can be handled by yet other agents, 5 and 6.

Figure 8.13b depicts a situation in which agent 4 terminates its work because of a hardware failure and another agent with the same competences takes over. Finally,

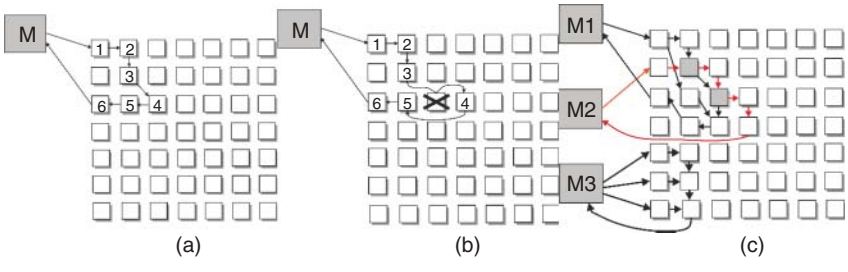


**Figure 8.13** Different types of team formation in the flat network of Figure 8.12 (a).

Figure 8.13c shows a configuration in which there are a number of parallel tasks injected by several mandators (which is the normal case), and permanent negotiations take place between all agents in the network for performing the subtasks. Agents used sequentially in processing more than one task are shaded in gray.

In this example, agents 1, 2, and 3 are responsible for information processing in the PMG. They could be replaced easily by other information processing agents in the network that can perform the same tasks, depending on their workload. Clearly, one could even think of a completely centralized solution, where all of the information collection and data management is done in a remote data center outside the PMG. This would, however, violate the principle of autarky, would cause much more traffic, would be less resilient in high load situations, and would be much more vulnerable to network component failures, and so on. Nevertheless, a limited hierarchy could be a viable alternative, where one centralized top-level agent per PMG is the single entry point for all tasks, and a number of equally competent agents for one (sub)task class would be below this agent (this would be the situation according to Figure 8.13b).

To compare these two situations from an information processing perspective, we have conducted extensive simulations with a large number of parameters. These parameters included (among others) the network size $K$, a required fixed deadline for a given task, the completion probability $V$ (the percentage of tasks successfully completed before a given deadline), the probability $b$ of an agent accepting an offered task, the failure probability $f$ (of an agent being unable to complete the task), and the repair delay $r$ (time after an agent failed to resume its work).

We conclude by looking at one result: the performance of the network when reconfiguration is necessary because of the failure of individual nodes. Figure 8.14 illustrates the effect of increasing the network size $K$ and varying the failure probability $f$, which was 0.01 and 0.05, in Figure 8.14a,b, respectively. In addition, the performance of flat (fl) and hierarchical (hi) organizations are

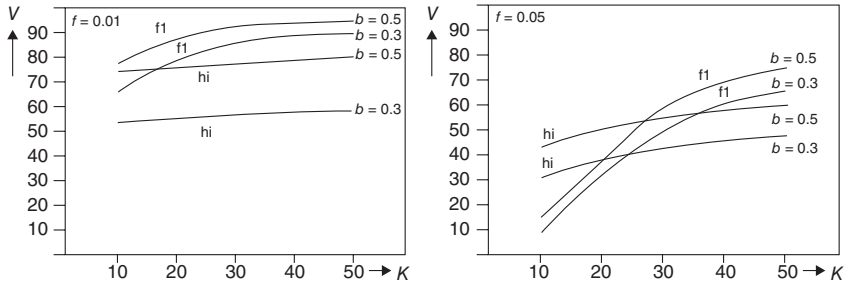


**Figure 8.14** Simulation of the two network topologies fl(at) and hi(erarchical). The graphs show the effect of network size $K$ on throughput $V$ with two varying acceptance probabilities $b$. There are two varying parameters: network structure and completion probability. (a) Low failure probability $f = 0.01$ and long repair delay $r$. (b) Same parameters but high failure probability $f = 0.05$ and long repair delay $r$. The repair delay in these cases is 10 times longer than the required completion deadline.

shown for different degrees of task acceptance probabilities $b$ (the reciprocal of task complexity). In the case of low failure probability $f$ (Figure 8.14b) fl is superior to hi: even with small network sizes, fl provides a higher percentage $V$ of tasks completed successfully than hi. This advantage increases with growing network size $K$ because the set of potential agents that a mandator may select from becomes larger in the case of fl. This is also true in the case of high failure probability. Here, too, a larger network size will increase the likelihood of finding a working agent, reducing the average amount of time needed for repeated futile negotiation phases. Moreover, in a larger network an increase in complexity ($b$ getting smaller) results in less degraded performance for fl when compared to hi. Nevertheless, we note that with small network sizes, hi shows a better performance than fl. Still, as $K$ increases, a break-even point is reached, at which fl's performance exceeds that of hi.

A more detailed analysis is beyond the scope of this chapter, but the modeling tool and the simulation with a very rich parameter set make it possible to design autonomous energy systems with very high precision with respect to a desired target by looking at various scenarios. However, even the presented analyses show that there are many ways of organizing a complex network of interdependent communication and energy flows – and that there is *no* "one-architecture-fits-it-all" approach to setting up these systems. Nevertheless, if there is a certain degree of redundancy in the hardware structures and the communication pathways are sufficiently developed to handle protocols such as the contract net protocol, the control software can provide an unprecedented degree of flexibility!

## 8.3 The Big Picture

### 8.3.1 Centralized versus Decentralized Systems

A critical endeavor for researchers in the field of energy systems is to transform our energy landscape toward a sustainable and green future. Based on the existing energy storage technologies, we believe that we need not only a restructuring and decentralization of the electricity production, but also a whole new architecture of the energy system in order to tap the full potential of smart production, transportation, and storage of electricity. As will be shown later, the establishment of quasi-autonomous energy clusters can be a solution to reduce the need for grid extension considerably.

Given the rapid development of renewable energy we are currently facing, there are two design approaches one could pursue in the structuring of our energy system: The top-down approach (i) is to construct large-scale wind parks and photovoltaic (PV) sites, and to heavily invest in grid extension for the transport of electricity to the consumer and the increase of the storage capacity of the grid. This approach will most probably lead to the fulfillment or even over-fulfillment

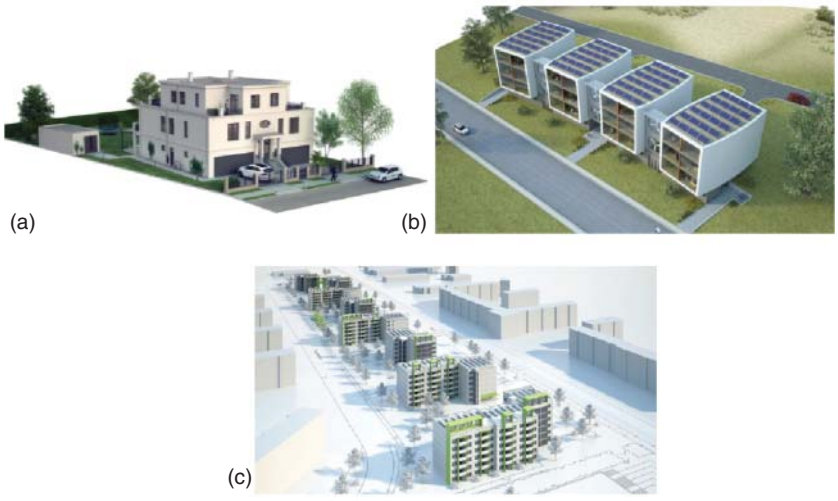


**Figure 8.15** Scalability of energy clusters by choice of technology from single homes (a), to blocks (b), to districts (c). (Reprinted from Ref. [12].)

of the obligations for electricity production on the way to a completely renewable energy supply by 2050. However, in this scenario effective energy management is restricted to a limited number of large-scale storage technologies, such as pumped-storage power plants and compressed air storage sites. In addition, grid extension to that extend can be quite costly.

In contrast, the bottom-up approach (ii) favors self-sustaining and largely autonomous energy clusters together with a need-based, local production of electricity. By this, one could minimize the need for energy storage and greatly reduce supplementation from the grid. With the right choice of technology for energy conversion and storage, those energy clusters could range from single-family homes to city blocks or even whole districts, production sites, and small remote villages (see Figure 8.15). All of this demands the development of an efficient management structure, hereafter referred to as *computational energy science*, under which those energy clusters can act as quasi-autonomous microgrids. A novel architecture of the energy system based on energy clusters could focus on the combination of multiple small-scale technologies to design generation, storage, and consumption in a smart way. Figure 8.16 depicts what an energy cluster within the smart grid could look like. In Chapter 2 some governing principles were described; see also Figure 8.5.

### 8.3.2
### Decentralized Energy Systems: a Closer Look

In a decentralized energy system the energy production facilities are located closer to the sites of energy consumption. The key point of a decentralized energy system is that it allows for more optimal use of renewable energy as well as combined

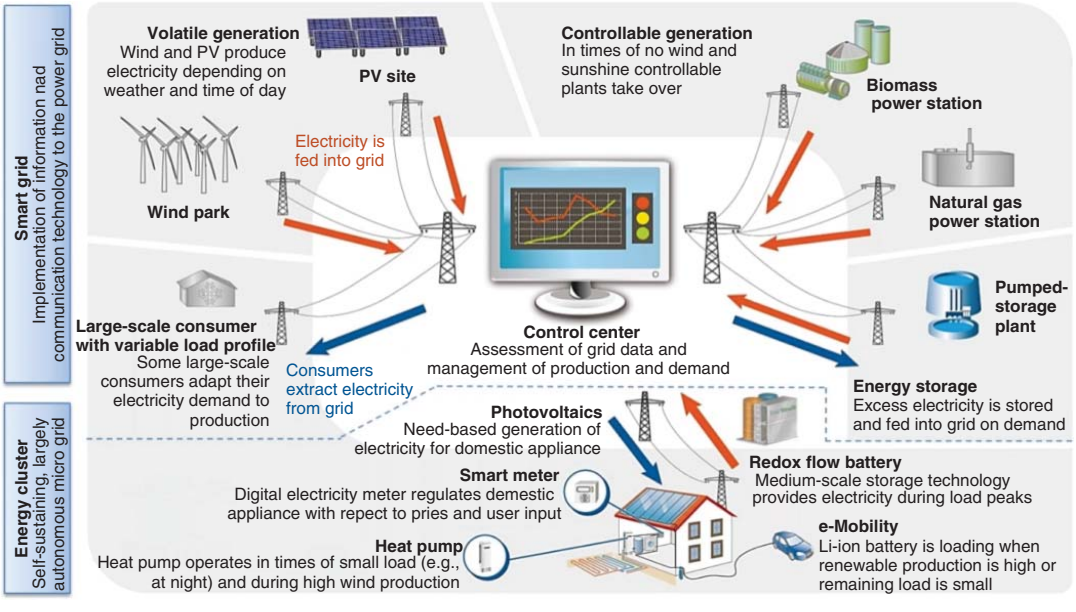


**Figure 8.16** Smart grid architecture featuring autonomous energy cluster. (Rearranged from Ref. [13].)

heat and power, simultaneously reducing fossil fuel use and increasing overall eco-efficiency. The use of decentralized energy systems is a relatively new methodology in the power industry in most countries. Traditionally, the power industry focuses on developing large, central power stations where the power is generated and then transmitted across long distribution lines to sites of consumption. On the other hand, decentralized energy systems seek to put power sources closer to the end user. Sourcing energy generation in a similar decentralized manner as that of the end users can reduce the transmission and distribution inefficiencies, and the related economic and environmental costs.

A decentralized system relies mainly on distributed generation and energy storage. The primary element of a decentralized energy system is distributed generation, also known as *on-site generation*. Although both heat and electricity can be generated in a decentralized system, only electricity can be transported over larger distances while heat needs to be consumed within some 10 km. Switching to decentralized power generation allows for heat and power generation coordination in combined heat and power plants, for example, by using fuel cells. This in turn results in increasing the system's efficiency because heat is a by-product of many electricity-generating techniques.

The use of more than one generation of sources in a decentralized system may lead to new difficulties in controlling supply to best match demand. However, storage techniques such as batteries, compressed air, and pumped hydro storage can help in storing energy when supply exceeds demand and feeding it back into the

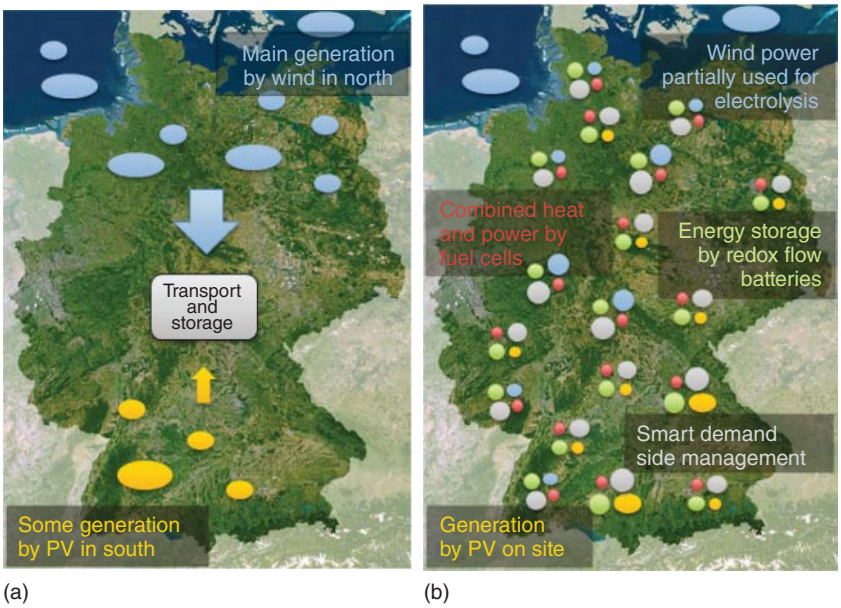


(a) (b)

**Figure 8.17** Possible scenarios for layouts of centralized (a) and decentralized energy systems (b) in Germany.

grid during peak hours. Storage is particularly useful for intermittent renewable energy plants, which often produce electricity at their highest capacities during nonpeak hours. In the next section, we give a brief overview of the main storage devices that can be integrated into a decentralized energy system.

Figure 8.17 shows a comparison between a centralized energy system (Figure 8.17a) and a decentralized energy system (Figure 8.17b) in Germany, where the latter offers a combination of multiple small-scale technologies to design generation, storage, and consumption in a smart way. The decentralized energy system is characterized by the generation of electricity where it is needed, and a minimum need for energy storage and minimal supplement from the grid.

## 8.4 Storage Components

### 8.4.1 How to Store Energy

The technical performance of energy storage devices is mainly described by four key parameters. The energy density (i) is the amount of energy stored in a system of given mass (gravimetric) or a region of space (volumetric), while the power of an energy storage device per mass or volume is referred to as the power density (ii). The time of energy storage characteristic for a specific device design is called storage time (iii), and internal reactions, which reduce the stored charge in a device without any load connected in the external circuit is the so-called self-discharge (iv).

The above-described criteria apply to different technical realizations of energy storage systems. One generally distinguishes between thermodynamic energy storage devices that store energy as latent heat and electrical energy storage devices that allow multiple ways of energy conversion. A representative of the first category is building material featuring micro-encapsulated phase change materials (PCMs) that absorb heat when they change from solid to liquid and release heat and vice versa [14]. The second category is represented by (super-) capacitors (energy stored in electric fields), batteries (energy stored in the charge state of single molecules within an encased system), or flywheels and pumped-storage power plants (energy stored mechanically). Furthermore, chemicals (such as hydrogen) can be used for long-term energy storage in combination with converters (e.g., fuel cells).

Figure 8.18 puts several battery-related technologies into context with electrical and mechanical energy storage devices. In general, electrochemical energy storage possesses a number of desirable features, including pollution-free operation, high round-trip efficiency, long cycle life, low maintenance, as well as flexible power and energy characteristics to meet different grid functions (like load leveling and power quality management) [15]. Therefore, the next section focuses on some of the most relevant electrochemical energy storage systems.

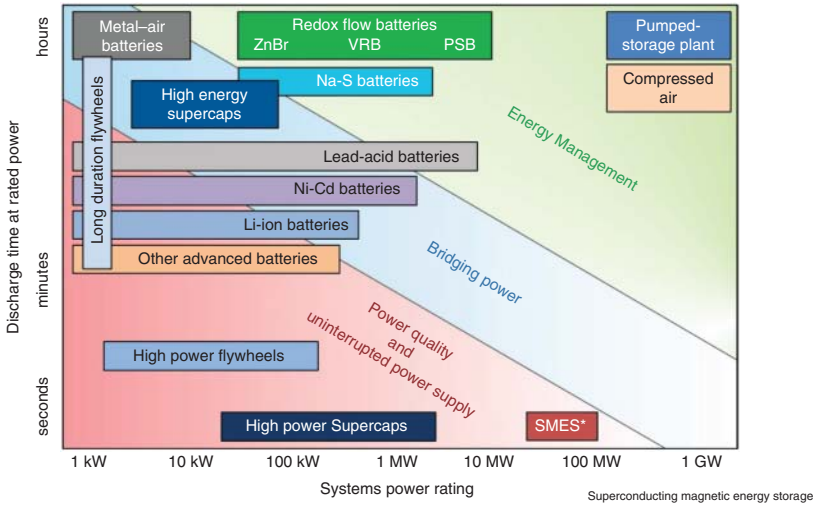


**Figure 8.18** Comparison of power rating and discharge time for various energy storage systems.

### 8.4.2 Selected Energy Storage Devices

Electrochemical energy storage devices can be classified in terms of their diverse operating principles. Regardless of their specific internal chemistry, batteries store energy through charge transfer reactions within their electrode structure. Redox flow batteries (RFBs), in contrast, possess storage tanks containing redox species that are continuously circulated through the cell under change of their charge state. In supercaps, an electrical double-layer arises at the electrode/electrolyte interface, that is, energy is stored in the electric field between spatially separated charges. Consequently, supercaps could be categorized as both electrochemical and pure electrical energy storage devices. Finally, fuel cells represent yet a different, non-rechargeable kind of electrochemical storage system, since the energy is stored in the reactants (hydrogen, ethanol, etc.) that are externally fed to the device.

#### 8.4.2.1 Li-Ion Batteries

Figure 8.19 compares a state-of-the-art Li-ion battery pack used in battery electric vehicles (BEVs) with a standard lead–acid car battery. The mature scientific approach of Li-ion technology to intercalate $Li^+$ ions into host structures outperforms conventional batteries in terms of energy and power density, no matter what battery chemistry it is compared to (see Table 8.1). The reaction mechanism is summarized in Eq. (8.1).

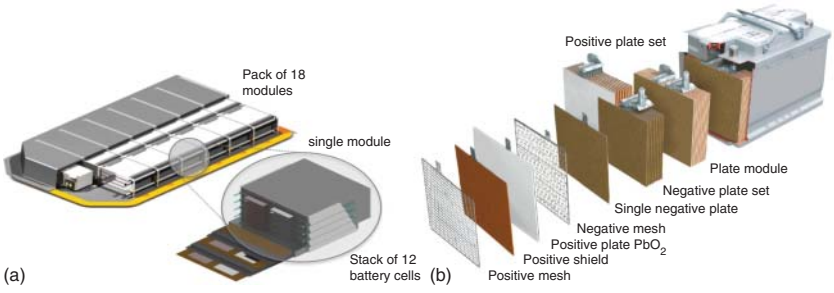


**Figure 8.19** (a) Li-ion battery pack comprised of 216 single cells in 18 modules [16] and (b) standard lead–acid car battery.

**Table 8.1** Key parameters of state-of-the-art batteries with different chemistries [17].

| Battery type | Pb | Ni–Cd | Ni–MeH | Na–S/Na–$NiCl_2$ | Li-ion |
|---|---|---|---|---|---|
| Energy density volume ($Wh\,l^{-1}$) | 90 | 150 | 200 | 345/190 | 300–400 |
| Energy density gravimetry ($Wh\,kg^{-1}$) | 35 | 50 | 70 | 170/120 | 200–300 |
| Power density volume ($W\,l^{-1}$) | 910 | 2000 | 3000 | 270 | 4200–5500 |
| Power density gravimetry ($W\,kg^{-1}$) | 430 | 700 | 1200 | 180 | 3000–3800 |
| Self-discharge | + | + | + | – | ++ |
| Fast charging | – | ++ | + | – | + |

$$\begin{array}{c} Li^+ + e^- + 2Li_{0.5}CoO_2 \leftrightarrow 2LiCoO_2 \quad \text{(cathode)} \\ LiC_6 \leftrightarrow Li^+ + e^- + 6C \quad \text{(anode)} \\ \hline LiC_6 + 2Li_{0.5}CoO_2 \leftrightarrow 2LiCoO_2 + 6C; \quad \Delta U_0 \approx 4.1\ \text{V} \end{array} \tag{8.1}$$

In state-of-the-art rechargeable Li-ion batteries transition metal oxides serve as reversible cathode materials [18]. Lithiation of the transition metal oxides results in $LiMO_2$ compounds (in most commercial systems M = Co) that serve as the source of lithium in the cell. As an anode host structure that allows Li intercalation, most Li-ion battery types rely on graphite, whereas the standard electrolyte solutions are alkyl carbonate solvents.

Beyond the above-described graphite–$LiCoO_2$ system that powers most of today's portable electronic devices, such as laptops and cell phones, there is a new generation of Li-ion batteries that features novel anode and cathode materials. A compendious presentation of these advanced Li-ion battery concepts is far beyond the scope of this chapter and there are excellent reviews that provide a comprehensive overview of the recent developments [19]. However, one particular system shall be highlighted here, which renders Li-ion technology suitable for stationary applications, such as load leveling.

By introducing lithium titanate $Li_4Ti_5O_{12}$ (LTO) as a new anode intercalation material and combining it with highly stable $LiMPO_4$ cathodes, the resulting battery system exhibits very prolonged cycle lifetime, impressive stability, and excellent safety features [20, 21]. LTO electrodes are inferior to graphite in terms of their capacity, which leaves LTO-based batteries with rather low energy density. However, in terms of load leveling applications for which energy density is not important, LTO electrodes seem highly suitable, because they are very fast and excel in low temperature performance [22]. At the redox potential of this electrode there are no major reduction processes of standard electrolyte solutions. Because of this fact, LTO electrodes exhibit very prolonged cycle life. As a family of cathode materials $LiMPO_4$ and especially its representative $LiFePO_4$ feature a practical capacity that almost reaches the theoretical one (165 out of 170 mAh $g^{-1}$). It furthermore possesses an excellent rate capability even at low temperatures and very good safety features. As another decisive advantage, it is much less thermally active with standard electrolytes than lithiated transition metal oxides. Prototype cells employing the upper combination of novel anode and cathode materials represent impressive demonstrations of how Li-ion technology can contribute to the storage of renewable energy.

#### 8.4.2.2 Post Li-Ion Batteries

Apart from the long-commercialized Li-ion battery concept, significant research effort is put into Li–S and Li–air systems, the so-called post Li-ion batteries. For use in BEVs the theoretical energy density of Li-ion batteries (387 Wh $kg^{-1}$) is too low to approach the desired driving range of ~500 km between charging [23]. The move from Li-ion to Li–S and Li–air would represent a great leap forward in terms of energy density. The reaction products on the cathode side, namely $Li_2S$ and $Li_2O_2$, store more lithium and hence more charge per unit mass, than $LiCoO_2$. On the anode side lithium metal stores more charge per unit mass than Li-intercalated graphite electrodes. Figure 8.20 depicts a schematic representation of Li–S and Li–air batteries, while Eqs. (8.2) and (8.3) provide the main reaction mechanisms.

$$\begin{array}{rr} S + 2Li^+ + 2e^- \leftrightarrow (Li_2S)_{solid} & \text{(cathode)} \\ 2Li \leftrightarrow 2Li^+ + 2e^- & \text{(anode)} \\ \hline 2Li + S \leftrightarrow (Li_2S)_{solid} & \Delta U_0 \approx 2.0\ \text{V} \end{array} \tag{8.2}$$

$$\begin{array}{rr} O_2 + 2Li^+ + 2e^- \leftrightarrow (Li_2O_2)_{solid} & \text{(cathode)} \\ 2Li \leftrightarrow 2Li^+ + 2e^- & \text{(anode)} \\ \hline 2Li + O_2 \leftrightarrow (Li_2O_2)_{solid} & \Delta U_0 \approx 4.1\ \text{V} \end{array} \tag{8.3}$$

In Li–S batteries, the Li–metal anode is oxidized upon discharge, releasing $Li^+$ into the electrolyte (vice versa upon charge). At the cathode, elemental sulfur is reduced upon discharge to form various polysulfides. These compounds then combine with $Li^+$ to form the final discharge product $Li_2S$ (on charging it is decomposed again to $S + 2Li^+ + 2e^-$).

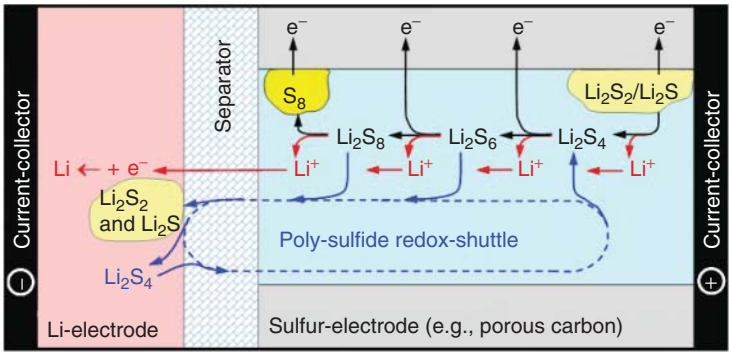


(a)

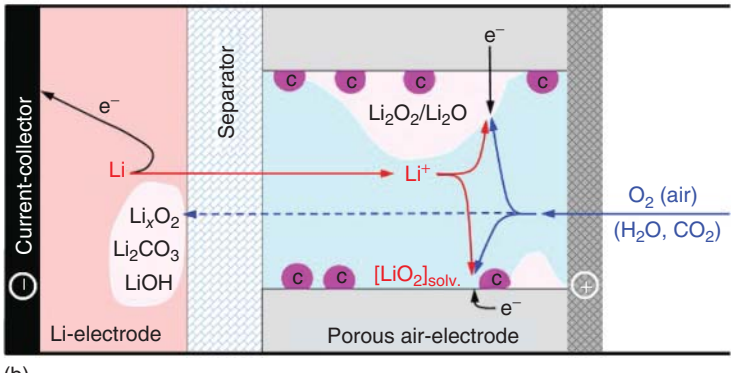


(b)

**Figure 8.20** Prinicple of Li–S (a) and Li–air battery (b) [24].

Li–S batteries represent a promising concept due to (i) the natural abundance and low cost of sulfur and (ii) the high theoretical energy density of 2567 Wh $kg^{-1}$ [25, 26]. However, major drawbacks that hampered the commercialization of Li–S technology are (i) the poor electrode rechargeability owing to the solid reaction product $Li_2S$ ("cathode clogging") and (ii) the diffusion of polysulfide intermediates $Li_2S_n$ ($3 \leq n \leq 6$) to the anode ("capacity fading").

In Li–air batteries, molecular oxygen $O_2$ from air enters the cathode's porous carbon structure. It dissolves in the electrolyte found inside the pores and is reduced to $O_2^{2-}$ upon discharge. In combination with $Li^+$, produced at the anode as in Li–S batteries, the final discharge product lithium peroxide $Li_2O_2$ is formed (on charging, it is decomposed again to $O_2 + 2Li^+ + 2e^-$).

Li–air batteries offer an even higher theoretical energy density than Li–S of 3505 Wh $kg^{-1}$. Among others, the most apparent problem of Li–air batteries, which they also share with polymer electrolyte membrane fuel cells (PEMFCs), is the oxygen reduction reaction (ORR). Until now, no research group has succeeded in the synthesis of a suitable ORR catalyst to replace high-cost noble metal catalysts such as Pt, Au, or Pd. The designing and preparation of highly

active non-noble metal cathode catalysts for Li–air batteries and PEMFCs is one of the most eagerly pursued targets of modern electrochemistry.

A common R&D challenge of both Li–S and Li–air technology is the poorly controlled Li/electrolyte interface at the anode side. An improved Li–metal anode design or an alternative material is a prerequisite for both systems to advance to maturity.

#### 8.4.2.3 Redox Flow Batteries

For energy storage in the medium scale (10 kW to 10 MW), RFBs offer a multitude of advantages over other technologies, such as flexibility (energy and power scale independently), depth of discharge, rapid response, instantaneous refueling, high cycle lifetime, and good safety features (nonhazardous materials). This renders RFBs a suitable device when it comes to applications such as load leveling or power quality control.

In typical RFBs, two external reservoirs contain soluble electroactive species. These are continuously circulated through the cell and undergo a reduction/oxidation process at the interface with the respective electrode. To maintain electroneutrality, an ion-selective membrane separating the positive and the negative redox species within the two flow compartments allows the transport of non-reaction ions, for example, $H^+$ [27].

Successful prototypes mostly rely on the all-vanadium chemistry with a $V^{2+}/V^{3+}$ redox couple in the negative compartment and the corresponding $V^{4+}/V^{5+}$ redox couple in the positive compartment [28]. Table 8.2 lists several other RFB chemistries and the corresponding cell voltage, efficiency, as well as energy and power density. Here, special focus shall be placed on a new concept featuring the so-called mega ions that contain multiple transition metal redox centers. Since the energy in RFBs is stored in the form of reduced and oxidized electroactive species in the electrolyte, the use of mega ions offers a great potential. Multiple redox states and the high number of electrons per unit volume could lead to considerably higher energy and power density than in conventional RFBs. Under electrochemical analysis, mega ions have been proved to exhibit fast

**Table 8.2** Main parameters for the characterization of different redox flow battery chemistries.

| Redox couple | $\Delta U_{cell}$ (V) | Overall efficiency (%) | Energy density (Wh $l^{-1}$) | Power density[a] (W $m^{-2}$) |
|---|---|---|---|---|
| Iron–chromium | 1.2 | 95 | 13–15 | 200–300 |
| All-vanadium | 1.6 | 83 | 25–35 | 600–700 |
| Vanadium-bromide | 1.4 | 74 | 35–70 | 220–320 |
| Mega-ions | 1.5 | 96[b] | 250[c] | 2000 |

a) Estimated as measured current density times cell voltage.
b) Coulomb efficiency of half-cell.
c) Estimated value based on solubility of 1 mol $l^{-1}$ and six electrons per redox molecule [29].

and reversible multielectron redox activity [29]. Besides, their application in RFBs and also in supercaps could possibly benefit from the advantageous properties of mega ions. However, RFBs and supercaps relying on mega ions have not reached a state beyond laboratory status.

### 8.4.3 Application to a City Block

In an exemplary simple calculation, we want to outline the capabilities of such energy clusters in terms of need-based production and autonomy. The energy cluster we consider in the following is a $100 \times 100\,m^2$ five-story city block in Munich, Germany, with a net floor space of $9000\,m^2$ (see Figure 8.21). The first floor is assumed to accommodate shops and service industry with an average electricity consumption of $100\,kWh\,(m^2\,a)^{-1}$ [30]. From the second to the fifth floor two-person apartments will be established. Assuming a standard size of $80\,m^2$ per apartment, the contemplated four stories provide space for 450 apartments. Under consideration of an average electricity consumption of $2500\,kWh\,a^{-1}$ for a two-person household the total electricity demand of the energy cluster amounts to $2\,025\,000\,kWh\,a^{-1}$ [30].

On the generation side, a multitude of renewable energy converters comes into play; all estimates are based on the typical climate situations of Munich, Germany. The roof area of $9000\,m^2$ can be equipped with panels of advanced

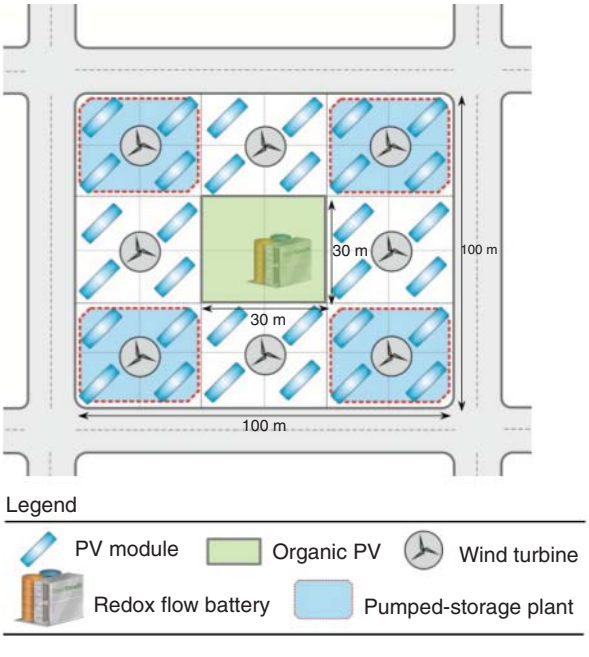


**Figure 8.21** Largely autonomous city block as example for energy cluster.

monocrystalline solar cells that nowadays possess an efficiency of more than 20% [31]. Presuming an irradiance of 1000 kWh $(m^2a)^{-1}$, an air mass of 1.5, and a flat roof with an orientation of the panels toward the south, and taking into account 25% of losses (due to shadowing, snow coverage, reflection, etc.) a PV generation of 1 350 000 kWh $a^{-1}$ is feasible [32]. Furthermore, organic PV covering the inner yard of the building can produce 75 000 kWh $a^{-1}$, implying the same parameters as before and an efficiency of 10% [31]. An additional installation of eight house wind turbines with a power of 10 kW per turbine and 2000 full load hours per year could contribute 160 000 kWh $a^{-1}$. In total, the on-site generation of the energy cluster sums up to 1 585 000 kWh $a^{-1}$.

In consequence, only a difference of 440 000 kWh $a^{-1}$ cannot be produced by the cluster itself and has to be supplemented from the power grid or by other kind of decentralized power production (e.g., by fuel cells). This is equal to 22% of the total consumption.

Besides energy demand and generation, the third pillar that the energy cluster is based on is energy storage. An ambitious goal would be to store 30% of the daily consumption, in order to account for the volatility of renewables. Upon the installation of four small-scale pumped-storage units with a volume of $10^6$ l each, the height of 15 m from the top floor to the basement of the building results in a storage capacity of 220 kWh. An advanced RFB featuring an energy density of 0.25 kWh $l^{-1}$ (this is based on the possibly achievable energy density using mega ions) would be a suitable energy storage device to store the remaining 1440 kWh. For this scale of application, the electrolyte storage tanks would need to contain 5760 l of electrolyte, which is a reasonable size for stationary devices.

All in all, the results of this assessment render energy clusters a self-sustaining and largely autonomous element of novel energy architectures. In case of a completely autonomous cluster where a supply of the residual electricity through the grids is not feasible or not desirable, additional systems with a high availability need to be set up. One such system that uses a fuel that has very low carbon footprints is the DEFC. Ethanol can be produced from organic waste, which is plentiful and does not interfere with the food chain. In the next section, we discuss DEFCs as an energy conversion supplement and how it fits in the big picture of decentralized energy systems.

## 8.5 Conversion Components, DEFC

### 8.5.1 Introduction to DEFC

Fuel cell technology promises to sustainably change electrical energy production by being significantly more efficient and environmentally friendly than the traditional combustion of fossil fuels. Fuel cells are electrochemical devices that

convert chemical energy to electrical energy through electrochemical reactions and so they are not limited by the Carnot efficiency.

The basic operation of a hydrogen fuel cell is fairly simple, being the reverse of water electrolysis [33]. PEMFCs are generally considered to be among the most advanced fuel cell technologies. In a PEMFC, hydrogen is oxidized (reaction (8.4)) by a platinum (Pt) electrocatalyst at the anode, generating electrons and protons. The protons migrate through a proton-conducting membrane toward the cathode, which is also composed of Pt or Pt-based alloy, while the electrons move to the cathode through an external circuit, generating usable electricity. Reacting with protons and electrons at the cathode, oxygen is reduced (reaction (8.5)), thereby forming clean water. PEMFCs are well suited for portable and microdevices, as well as for automotive applications.

$$2H_2 \rightarrow 4H^+ + 4e^- \tag{8.4}$$

$$O_2 + 4e^- + 4H^+ \rightarrow 2H_2O \tag{8.5}$$

Most research in fuel cells for use as portable power has employed PEMFCs. For low-temperature (~90 °C) PEMFCs running on hydrogen, the hydrogen can be generated from electricity via electrolysis of water, but this process suffers from the low system efficiency (60–73%) of commercial electrolyzers [34]. On the other hand, hydrogen could be reformed from hydrocarbons and alcohols (e.g., methanol or ethanol) on board. While hydrogen production is common place in the chemical industry and some interesting biotechnological advances were made [35, 36], it is more demanding for mobile applications because of issues such as weight, size, transient operation, and consumer safety [37]. Moreover, low-temperature PEMFCs require a supply of almost pure $H_2$. Especially, the CO content in the fuel has to be low (<20 ppm) to avoid poisoning of the anode catalyst [38]. In order to obtain hydrogen with such purity, selective processing that involves multiple reforming steps and cleaning are necessary (Figure 8.22; Path 1), if it is reformed on board [39]. While demonstrator vehicles with on-board reforming were realized, Daimler Chrysler's Necar 5, for example, featured a very sophisticated methanol reformer [40]; the high degree of integration required is demanding and also leads to high costs [41]. The array of fuel processors that is necessary to extract hydrogen from hydrocarbons was referred to as a *mobile small chemical plant* [41]. Operating a PEMFC on hydrogen but at 160 °C does not require the use of ultra-pure hydrogen because the catalyst poisoning by CO is not an issue at this temperature, and therefore many of the steps shown in Path 1 of Figure 8.22 are not required. This results in a simpler reforming process represented in Figure 8.22 by Path 2.

In direct PEMFC systems the fuel is oxidized at the surface of the electrode without reforming, which allows for a simpler design (Figure 8.22; Path 3). Over the last 40 years, there has been extensive research on direct methanol fuel cells (DMFCs) for portable power applications at low to moderate temperatures [42–44]. However, there are a number of problems associated with the use of methanol as a

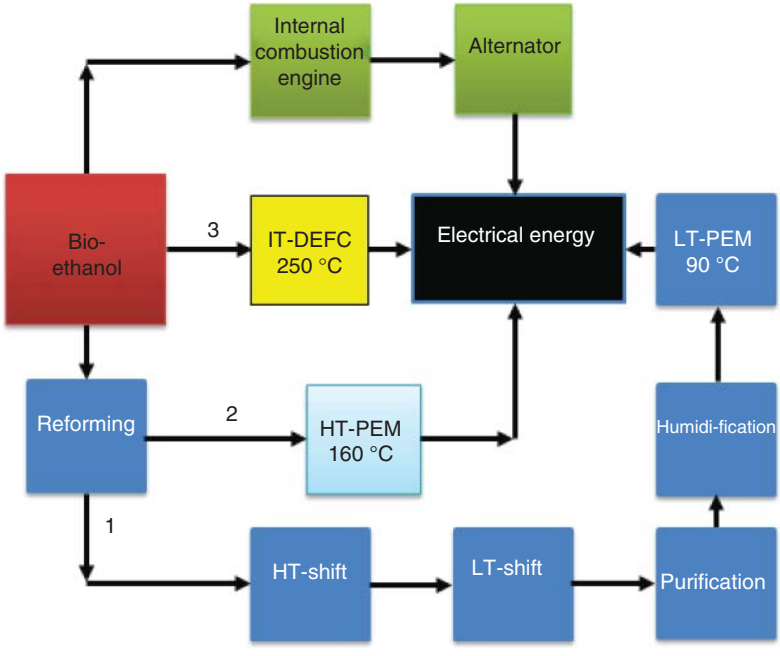


**Figure 8.22** A diagram showing the possible pathways of using ethanol as a fuel. IT, intermediate temperature; HT, high temperature; LT, low temperature; PEM, polymer electrolyte membrane.

fuel for portable power supplies. Methanol is highly toxic and could lead to long-term environmental problems because methanol is miscible with water [45]. These limitations have led researchers to investigate other fuels. Ethanol is an attractive alternative to methanol as a fuel. Ethanol is a renewable fuel and can be produced from farm products and also from organic waste. Ethanol and its intermediate oxidation products have been shown to be less toxic than other alcohols. Ethanol also can be disseminated via the existing infrastructure and it does not require advanced mobile storage containers as is the case with compressed or liquefied $H_2$.

The problem with using ethanol as a fuel (in comparison to methanol) is that complete oxidation of ethanol requires the breaking of a C–C bond, which is difficult at traditional Pt-based catalysts. This typically leads to incomplete oxidation of ethanol, which decreases the efficiency of the fuel cells and could provide toxic by-products or electrode passivation. Also, the reaction mechanism of the ethanol oxidation is not straightforward, and we will review the current knowledge of the reaction pathway both in acidic and alkaline media. The related question of a suitable membrane for intermediate temperatures will be also addressed. We also present methods of model catalyst studies to the ethanol oxidation reaction both in alkaline and acid media to take stock of what has been done so far to improve the catalytic activity toward the total oxidation of ethanol.

### 8.5.2 Ethanol versus Other Fuels

The use of ethanol as an alternative fuel to petroleum is associated with both great advantages and disadvantages [46]. Unlike petroleum, ethanol can be a renewable resource; it burns more cleanly in air than petroleum, producing less carbon (soot) and carbon monoxide. The use of ethanol as opposed to petroleum could reduce carbon dioxide emissions, provided that a renewable energy resource is used to produce crops required to obtain ethanol and to distil fermented ethanol. Another source is organic waste, which can be converted to ethanol. The disadvantages of using ethanol as a fuel are not trivial; some of these disadvantages include the lower heat of combustion (per mole, per unit of volume, and per unit of mass) compared to petroleum, and the large amounts of arable land required to produce the crops required to obtain ethanol, leading to problems such as soil erosion, deforestation, fertilizer run-off, and salinity. All these problems can be circumvented when using waste as the resource for ethanol. Internal combustion engines require some modification to use high concentrations of ethanol, but this has been shown in Brazil to be feasible.

For fuel cell applications, ethanol is becoming a more attractive fuel than both hydrogen and methanol due to its high mass energy density and the possibility of producing it in great quantities from biomass [47]. In addition, ethanol is less toxic than methanol and easier to handle than hydrogen [48, 49]. The use of ethanol as fuel has several advantages in comparison to hydrogen: it is a rather inexpensive liquid fuel, easy to handle, to transport, and to store, and with high energy density.

In addition to the performance and efficiency of the DEFC device, the energy density of the fuel plays a very significant role in several practical applications, including transportation and portable power sources. It is also a crucial factor for stationary generation because it determines which infrastructure is appropriate for fuel distribution [50]. The term *energy density* is defined as the amount of energy stored in a given system or region of space per unit volume ($kWh\,l^{-1}$), or per unit mass ($kWh\,kg^{-1}$) (see above when discussing storage devices in Section 8.4.1).

Figure 8.23 shows the energy density of various fuels. The gravimetric energy density of pure ethanol is about one order of magnitude larger than that of pressurized hydrogen (e.g., at 200 bar). The gravimetric energy density of ethanol is about two orders of magnitude higher than that of Li-ion batteries and the volumetric energy density is an order of magnitude higher. The energy density of ethanol is somewhat lower than that of conventional fuels, such as diesel fuel and gasoline.

### 8.5.3 Indirect versus Direct Ethanol Fuel Cell

Ethanol as fuel can be supplied directly to the anode side of a PEMFC for direct electrochemical oxidation of ethanol in order to produce electrical energy; in this

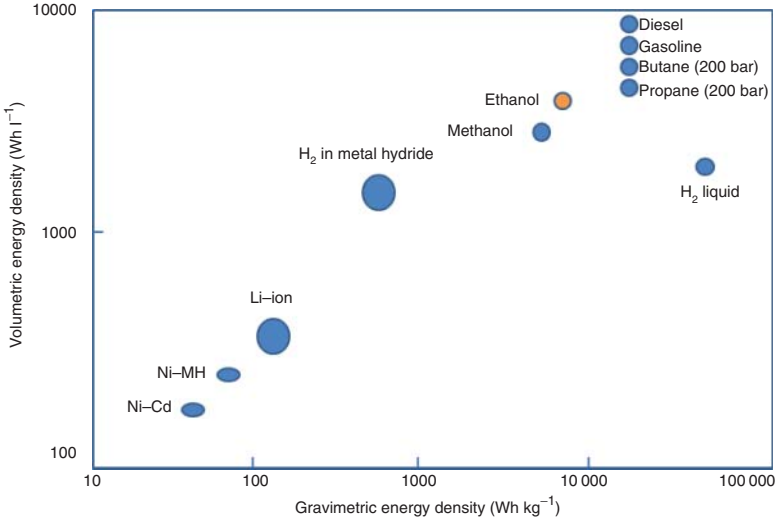


**Figure 8.23** Volumetric versus gravimetric energy densities of various fuels.

case, the device is called *direct ethanol fuel cell*. On the other hand, ethanol can be first reformed to extract hydrogen through an on-board reformer and the hydrogen gas is then supplied into a fuel cell (PEM) for the electrochemical oxidation of hydrogen at the anode producing electrical current. In the latter type, the fuel cell used is primarily a hydrogen fuel cell and ethanol is merely used as a source for hydrogen. There is a significant difference in the complexity between the direct and indirect ethanol fuel cells, as illustrated previously in Figure 8.22. A simple design for a DEFC system is shown in Figure 8.24.

The steam reforming of ethanol can provide up to 6 mol of hydrogen per mole of ethanol reacted:

$$CH_3CH_2OH + 3H_2O \rightarrow 2CO_2 + 6H_2 \quad \Delta H^o = 173.4\,KJ \cdot mol^{-1} \tag{8.6}$$

If the CO production is considered in the steam reforming of ethanol, the water gas shift reaction must be taken into account. The overall process, then, will be a combination of both reactions:

$$CH_3CH_2OH + H_2O \rightarrow 2CO + 4H_2 \tag{8.7}$$

$$CO + H_2O \rightarrow CO_2 + H_2 \tag{8.8}$$

The ethanol reforming process has a high-energy requirement, and occurs at a temperature of 650–700 °C, which is much higher than the typical operating temperature of a PEMFC. In addition, fuel processing on board including the reforming and cleaning stages adds to the size and weight of the fuel cell system, increases the complexity of the system for integration, slows down the system response time,

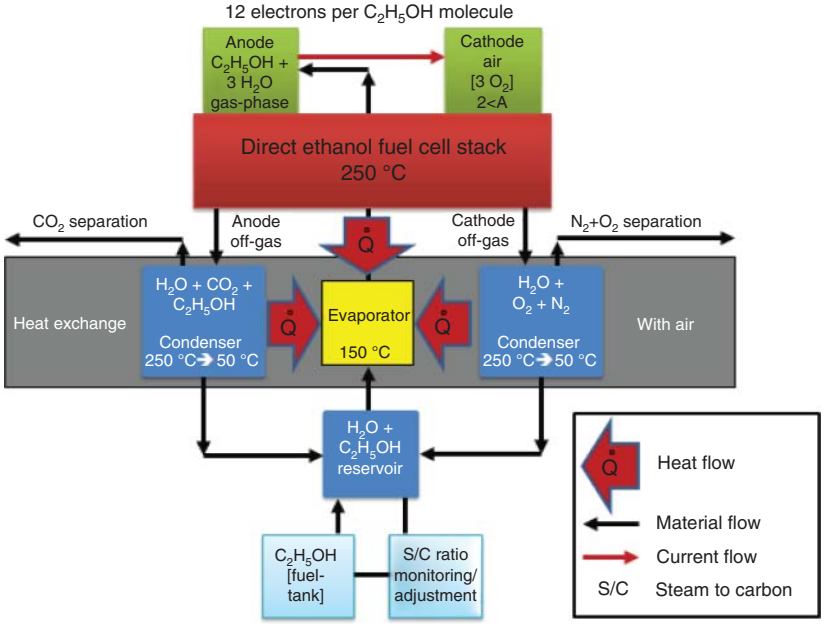


**Figure 8.24** System layout for direct ethanol fuel cell. No reforming is necessary that makes a compact design feasible. Solid arrows represent material flow.

and adds extra maintenance requirement. For all the aforementioned reasons, onboard fuel reforming is feasible but undesirable.

#### 8.5.3.1 Effect of Temperature on DEFC Performance

One of the key parameters of a DEFC is the cell performance. The operating temperature has a significant effect on the overall performance of DEFCs. Figure 8.25 shows a comparison between the cell performances when ethanol is directly fed as the fuel in two different fuel cell systems, that is, solid oxide fuel cell (SOFC) and PEMFC. One can clearly distinguish that the direct ethanol SOFC exhibits a superior performance to the direct ethanol PEMFC. In the former case, the maximum power is ~800 mW $cm^{-2}$, which is almost 10 times higher than that of the direct ethanol PEMFC at lower temperatures. This is mainly due to the much higher SOFC's operation temperature (800 °C) than that of the PEMFC (90 °C) [51].

#### 8.5.3.2 Stack Hardware and Design

A single DEFC includes only one anode and one cathode; therefore, the theoretical operating voltage of a single cell is 1.145 V (see reactions (8.6)–(8.8)), and the actual voltage in operation is lower than 0.9 V due to various types of voltage losses. In reality, the operating voltage can be as small as 0.7 V when drawing a useful current. This means that to produce a useful voltage, many cells have to be connected in series. Such assembly of fuel cells in series is known as a *stack*. To connect various cells (each cell is composed of a membrane electrode assembly,

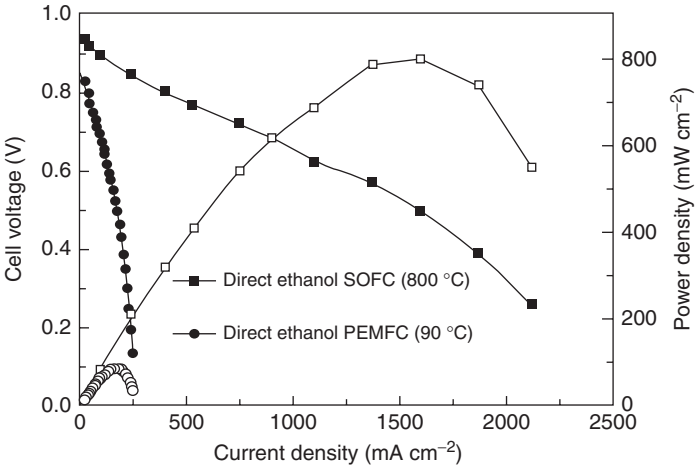


**Figure 8.25** Single cell performance comparisons between direct ethanol SOFC and direct ethanol PEMFC. Detailed operation conditions can be found elsewhere. (Reprinted from Ref. [51].)

MEA, and two gas diffusion layers, GDLs) together, a "bipolar plate" is used. Details regarding MEA fabrication and GDL functions are discussed in the next section. The use of a bipolar plate provides connections all over the surface of one cathode and the anode of the adjacent cell (hence "bipolar"), and hence they are made of a good conductor such as graphite or stainless steel. The bipolar plate also serves as a means of feeding oxygen to the cathode and fuel gas to the anode. These plates can have channels grooved into them so that the gases can flow over the face of the electrodes.

$$\text{Anode}: \quad C_2H_5OH + 3H_2O \rightarrow 2CO_2 + 12H^- + 12e^- \quad U_o = 0.085 \text{ V} \tag{8.9}$$

$$\text{Cathode}: \quad O_2 + 8H^+ + 8e^- \rightarrow 4H_2O \quad U_o = 1.230 \text{ V} \tag{8.10}$$

$$\text{Total}: \quad C_2H_5OH + 3O_2 \rightarrow 3H_2O + 2CO_2 \quad \Delta U_o = 1.145 \text{ V} \tag{8.11}$$

The first step in designing a fuel cell stack is to determine its active area (or the cell cross-sectional area) and the number of cells required in the stack. The design inputs come from the application requirements of the stack; these include, but are not limited to, the desired power output, desired or preferred stack voltage or voltage range, and volume and weight limitations. Some of these requirements may conflict with each other, so the stack design process often results in a compromise solution that meets the key requirements (such as power output) and finds an optimum between the conflicting requirements (Figure 8.26).

In Section 8.6 some of the materials important for a DEFC are discussed.

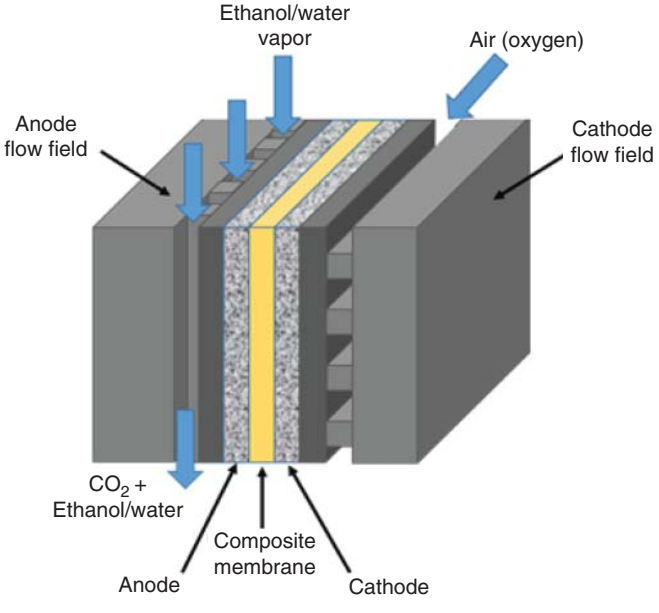


**Figure 8.26** Principle layout of a direct ethanol fuel cell (DEFC) at elevated temperatures.

## 8.6
## Materials and Molecular Processes

The discussion in this chapter follows in large parts [52].

### 8.6.1
### DEFC Components

We now focus on the molecular scale and how the electrochemical processes occur at the catalyst surface. This understanding lays the ground to developing a fuel cell. It determines what the best operating conditions are and what materials to choose to accomplish this.

The core of present DEFCs is a polymer electrolyte ion exchange membrane. The main function of the membrane in DEFCs, as well as in all PEMFCs, is to transport protons from the anode to the cathode and keep the fuel and oxidant separated, which prevents their direct reaction, which would be a chemical short circuit. Thus, the ideal polymer must have excellent proton conductivity, high mechanical strength, chemical and thermal stability, good flexibility, low gas permeability, and low cost.

The most common type of membranes uses a polymer, which is modified to include ions, such as sulfonic groups. These hydrophilic ionic species are the key for allowing proton transport across the membrane. Nafion® is one of the

most widely used membranes today; it is a polymer made for the first time by the DuPont company.

The electrodes (anode and cathode) are in direct contact with the membrane forming what is called *membrane electrode assembly* (*MEA*). The electrodes typically consist of two main layers: catalyst layer and GDL. The electrodes must be porous because the reactants are fed from the back side of the electrode and must reach the membrane (electrolyte)/electrode interface, where the electrochemical reactions take place in the catalyst layer, or specifically, on the catalyst surface. The catalyst layer is typically composed of a mixture of catalyst and Nafion ionomer. The catalysts that are typically made of Pt or Pt-based alloy at the cathode and anode, respectively, are in the form of nanoparticles supported onto high surface area carbon. The GDL is made of a mixture of carbon and PTFE polytetrafluoroethylene (Teflon) and its main function, due to its high porosity, is to facilitate the effective diffusion of reactants to the catalyst surface at the electrocatalyst layer. The GDL also forms the electrical contact between the electrocatalyst layer and the bipolar plate or other current collectors. Another important function of the GDL is that it helps in water management in the fuel cell as it carries the product water away from the electrolyte surface at the cathode side.

So far, the three components – membrane, electrocatalyst layer, and GDL – form a single fuel cell, but for practical aspects several cells are usually connected together in series to form a fuel cell stack. Bipolar plates are used to electrically connect the cells in series where the anode of one cell is connected to the cathode of the adjacent cell.

### 8.6.2 MEA and Electrodes

A fuel cell electrode is composed of a thin electrocatalyst layer pressed between the ionomer membrane and a porous, electrically conductive substrate (GDL). The electrocatalyst layer is a porous structure that usually consists of a matrix of high-surface-area carbon (used to disperse the electrocatalytic nanoparticles and connect them electrically to the current collector), small, high-surface-area catalyst nanoparticles (Pt-based alloy nanoparticles in case of DEFCs), and a binder, which is made of the same material as the polymer electrolyte membrane (PEM) (usually Nafion). The role of Nafion in the electrocatalyst layer is to transport protons from (to) the PEM to the electrocatalytic nanoparticles at the anode (cathode) where the electrochemical reaction takes place. The second function of the binder is to provide mechanical strength and adhesion to the electrocatalyst layer.

The GDL is typically a carbon fiber paper or carbon cloth and it does not participate in the electrochemical reactions but has several important functions. The GDL provides a pathway for the reactant gases flowing in the flow field channels to reach the catalyst layer allowing them to access the entire active area and not just to those adjacent to the channels. It also electrically connects the catalyst layer to the bipolar plate and provides mechanical support to the MEA, preventing it from sagging into the flow field channels.

The MEA is a combination of the two catalyst layers (anode and cathode) with the polymer membrane. There are two methods for the preparation of MEAs; the first way is to deposit the catalyst layer to the GDL, and then hot-press it to the membrane. This method is called *catalyst-coated GDL* (CCG). The second method, which is called *catalyst-coated membrane* (CCM), includes the application of the catalyst layers directly to the membrane, forming a so-called three-layer MEA or catalyzed membrane. A GDL may be added later, either as an additional step in MEA preparation (in that case a five-layer MEA is formed) or in a process of stack assembly. The catalyst layer may be added to the GDL or the membrane by many techniques, such as spraying, sputtering, painting, screen printing, decaling, electrodeposition, evaporative deposition, and impregnation reduction. Some of the lead manufacturers of MEAs are DuPont, 3M, and Johnson Matthey.

### 8.6.3 DEFC Processes

DEFCs are directly supplied with ethanol/water mixture at the anode side of the fuel cell. Ethanol is then directly oxidized producing carbon dioxide in addition to other possible by-products such as acetaldehyde and carbon monoxide and other small organic molecules. The formation of these by-products decreases the overall performance of the fuel cell and since some of them are hazardous they need to be avoided. The two half reactions and the overall reaction that occurs ideally in a DEFC equipped with a proton-conducting electrolyte are outlined below:

$$CH_3CH_2OH + 3H_2O \rightarrow 2CO_2 + 12H^+ + 12e^- \quad \text{(anode)} \tag{8.12}$$

$$3O_2 + 12H^+ + 12e^- \rightarrow 6H_2O \quad \text{(cathode)} \tag{8.13}$$

$$CH_3CH_2OH + 3O_2 \rightarrow 2CO_2 + 3H_2O \quad \text{(overall)} \tag{8.14}$$

In the case of an alkaline electrolyte, the reactions can be written as follows:

$$CH_3CH_2OH + 12OH^- \rightarrow 2CO_2 + 9H_2O + 12e^- \quad \text{(anode)} \tag{8.15}$$

$$3O_2 + 6H_2O + 12e^- \rightarrow 12OH^- \quad \text{(cathode)} \tag{8.16}$$

$$CH_3CH_2OH + 3O_2 \rightarrow 2CO_2 + 3H_2O \quad \text{(overall)} \tag{8.17}$$

#### 8.6.3.1 Ethanol Oxidation Reaction in Acidic Media

The ethanol oxidation reaction in acidic media follows a multistep reaction mechanism with a formation of by-products that reduces the electron yield. Some of these by-products adsorb on the catalyst surface leading to its deactivation [53, 54]. To elucidate the oxidation mechanism, ethanol oxidation in acidic media was investigated by several means including differential electrochemical mass spectroscopy (DEMS) [55–60], Fourier transform infrared spectroscopy (FTIR) [45,

53, 55, 61–63], gas chromatography (GC), high-performance liquid chromatography (HPLC) [64–67], and, more recently, liquid-state nuclear magnetic resonance spectroscopy (NMR) [68]. There is no one exact mechanism for the electrochemical oxidation of ethanol, as the mechanism, and ultimately the $CO_2$ yield, depend largely on catalyst composition, temperature, pressure, electrode potential, and even ethanol concentration. All the possible reaction intermediates and by-products, resulting from the electrochemical oxidation pathways of ethanol on 40 wt% Pt/C catalysts, were summarized in an extensive chart by Kim *et al*. [68].

In order to achieve a high activity for the ethanol oxidation reaction, that is, increase the $CO_2$ yield according to reaction (8.16), the C–C and C–H bonds need to be cleaved efficiently [59]; otherwise at least one of the partial oxidative reactions given in reactions (8.18)–(8.20) takes place:

$$CH_3CH_2OH \rightarrow CH_3CHO + 2H^+ + 2e^- \tag{8.18}$$

$$CH_3CH_2OH + H_2O \rightarrow CH_3CH(OH)_2 + 2H^+ + 2e^- \tag{8.19}$$

$$CH_3CH_2OH + H_2O \rightarrow CH_3COOH + 4H^+ + 4e^- \tag{8.20}$$

The formation of any of the by-products, acetaldehyde (Eq. (8.17)), ethane-1,1-diol (Eq. (8.18)), or acetic acid (Eq. (8.19)), is not desirable as it results in the decrease of the exploitable energy content of 8 kWh $kg^{-1}$ [57]. The formation of acetaldehyde or ethane-1,1-diol is associated with the release of 2 mol of electrons per mole of ethanol, while the formation of acetic acid is accompanied by four electrons, in contrast to 12 electrons in the case of $CO_2$ formation, which is the most desirable pathway.

The low reaction kinetics of ethanol oxidation is the major problem associated with using it as a fuel versus methanol oxidation [69] and so the efficiency of the system is quite different for ethanol than that for methanol. Methanol oxidation shows that carbon dioxide represents approximately 90% of products, whereas it varies between 20% and 40% depending on the catalyst material for ethanol oxidation [60].

When pure Pt is used as a catalyst for ethanol oxidation, studies showed that most of the ethanol was oxidized to acetic acid or acetaldehyde, and only a small fraction of $CO_2$ was obtained. The oxidation of ethanol on various catalysts composed of alloyed Pt with other transition elements showed an improvement in the catalytic activity [59, 70–72]. The most widely investigated materials for DEFC anode catalyst are the binary Pt–Ru and Pt–Sn and their corresponding ternary Pt–Ru-based and Pt–Sn-based alloys. The superior performance of these binary and ternary alloy electrocatalysts for the oxidation of ethanol with respect to pure Pt is attributed to the bifunctional effect [73] and/or to the ligand (electronic) interaction between Pt and alloyed metal(s) [73–75]. According to the bifunctional mechanism, the strongly adsorbed oxygen-containing species produced from the partial oxidation of ethanol, such as CO, can be released to make the Pt sites available for further ethanol adsorption in the presence of Ru

or Sn. Any of these two elements tends to form an ad-layer of oxygenated species (OH/O) at a much lower potential range with respect to that of Pt, and thus supply oxygen atoms at adjacent sites needed for the oxidation/and removal of the adsorbed oxygen-containing species on the Pt sites. The ligand effect postulates that the presence of Ru or Sn modifies the electronic structure of Pt, and, as a consequence, the adsorption of oxygen-containing species.

### 8.6.4 Anode Catalysts

PtRu alloys have become widely used electrocatalysts for DEFCs because it was found that alloying platinum with ruthenium helps increase the carbon monoxide tolerance of the platinum catalysts. Pt–Ru catalysts have also been used extensively for DMFCs and for hydrogen/oxygen fuel cells that employ contaminated hydrogen gas that is produced from a reformation process that may have carbon monoxide or carbon monoxide-like by-products.

The effect of temperature on ethanol electrochemical oxidation on Pt and Pt–Ru supported on carbon was investigated by cyclic voltammetry (CV) [76]. It was found that as the temperature increases from 25 to 80 °C, the CV results showed that Pt supported on carbon increased currents (i.e., electrocatalytic activity) by a factor of 4 only, whereas PtRu supported on carbon resulted in about an eight times increase in the electrocatalytic activity, for the same temperature range. The remarkable enhancement in ethanol oxidation by adding Ru to the Pt catalyst was attributed to the strong adsorption of OH on Ru.

The amount of Ru in the Pt–Ru catalyst has a very significant effect on the catalytic activity toward ethanol oxidation. Pt–Ru anode catalysts with atomic ratio (Pt:Ru) of 4 : 1 was found to have very poor activity for the electrochemical oxidation of ethanol at room temperature [77]. This poor activity can be explained by the insufficient Ru sites required to effectively assist the oxidation of adsorbed residues and thus the oxidation current (catalytic activity) remains almost at the levels obtained for pure Pt. Using cyclic voltammetry measurements, it was found that [78] the activity for the ethanol oxidation of Pt–Ru/C increases with the increase of the ruthenium content in the catalysts (range investigated up to Pt:Ru 1 : 3). An optimum Pt:Ru composition of about 3 : 2 was reported for the ethanol oxidation [79].

Figure 8.27 shows a comparison of fuel cell performance (polarization curves) for different alcohols oxidized on PtRu alloys as anode catalysts. It can be seen from the figure that the performance of a fuel cell running on methanol is better than those with all other alcohol fuels at high current densities. At a current density of 250 mA $cm^{-2}$, the cell voltage of a fuel cell running on methanol is 15%, 100%, and 700% higher than when ethanol, 1-propanol, and 2-propanol, respectively, are used as fuels [60]. At low current densities, the performance of DEFC is better than that with the other three fuels. This superior performance of ethanol at low current density is likely due to a decrease in crossover of ethanol versus methanol to the cathode through the polymer membrane. It is also interesting to

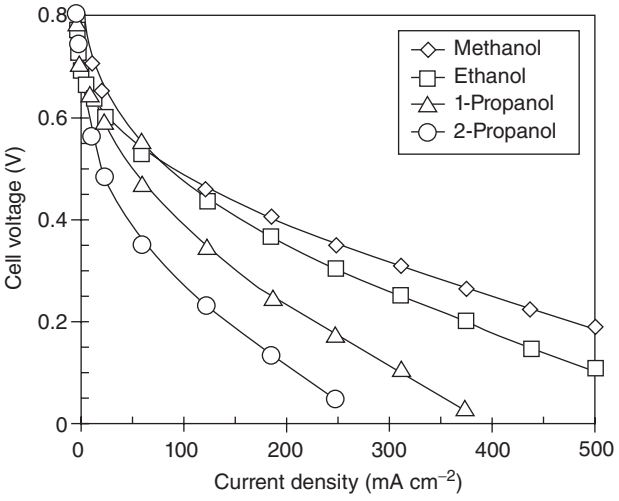


**Figure 8.27** Comparison of fuel cell performance for four different alcohol fuels employing a 4 mg cm$^{-2}$ Pt–Ru catalyst at the anode and a 4 mg cm$^{-2}$ platinum black at the cathode. (Wang *et al*. [60]. With permission.)

note that at the whole current density range the performance of propanol is significantly worse than that of methanol and ethanol. The oxidation of 1-propanol results in carbon dioxide and propionaldehyde, while the oxidation of 2-propanol forms carbon dioxide and acetone. It is worth mentioning that the direct alcohol fuel cells studied in Figure 8.27 are being operated at a high temperature of 170 °C [60]; an electrolyte membrane of polybenzimidazole was used as the temperature is too high for Nafion to be used.

#### 8.6.4.1 Pt–Sn as DEFC Anode Catalyst

Platinum and tin form five bimetallic intermetallic phases, $Pt_3Sn$, PtSn, $Pt_2Sn_3$, $PtSn_2$, and $PtSn_4$, of which $Pt_3Sn$ and PtSn are congruently melting compositions. These intermetallic phases are distinguished by distinct crystalline structures and unique X-ray diffraction patterns. Kuznetzov *et al*. [80] asserted that Pt forms nearly all possible alloys with Sn. Then, the shift of the fcc Pt peaks of Pt–Sn catalysts to lower angles than pure Pt but to higher angles than the fcc $Pt_3Sn$ phase should reveal the formation of a solid solution between Pt and Sn, due to the incorporation of Sn in the fcc structure of Pt. Radmilovic *et al*. [81], instead, attributed the value of the lattice constant of 0.3965 nm found for a commercial carbon supported Pt:Sn 1.23 : 1 catalyst, prepared by a conventional precipitation route by decomposing Pt and Sn precursors at 500 °C, to a mixture of $Pt_9Sn$ (0.3934 nm) [82] and $Pt_3Sn$ phases. Given the near-coincidence of the $Pt_9Sn$ and $Pt_3Sn$ reflections and the particle size broadening, a mixture of $Pt_9Sn$ and stoichiometric $Pt_3Sn$ would produce a diffraction pattern very similar to that of a nonstoichiometric $Pt_3Sn$ phase. Carbon supported Pt–Sn catalysts are commonly prepared in the absence of thermal treatment, and, as a consequence, are formed by an fcc Pt–Sn

alloy (or a mixture of $Pt_9Sn$ and $Pt_3Sn$ phases) and Sn and Pt oxides. The relative amounts of the Pt–Sn alloy and $SnO_2$ affects the electrochemical activity of these catalysts.

Conversely to DMFCs, DEFCs with Pt–Sn/C as anode material performed better than those with Pt–Ru/C [24, 39, 40], as shown in Figure 8.28. Song and Tsiakaras [49] compared the cell performances of DEFCs with various Pt–Sn/C (2 : 1) and Pt–Ru/C (1 : 1) catalysts as anode materials. As can be seen in Figure 8.28, the cells with Pt–Sn/C catalysts prepared by different methods performed better than the cells with commercial and in-house prepared Pt–Ru/C. In addition, Pt–Sn shows a much higher $CO_2$ efficiency, that is, a higher degree of complete oxidation than Pt–Ru catalyst [57].

#### 8.6.4.2 Ethanol Oxidation Reaction in Alkaline Media

The kinetics of methanol oxidation on Pt and PtRu was found to be one order of magnitude higher in alkaline media than that in acid solutions [83]. This is mainly due to the increased adsorption of $OH_{ads}$ on the catalyst surface, which helps oxidize the $CO_{ads}$ that is adsorbed on the Pt surface. As this oxygen-containing group is also of great importance for the ethanol oxidation reaction [68, 72, 84, 85], improved kinetics are expected for the anode reaction of alkaline direct ethanol fuel cells (ADEFCs). This notion is backed by density functional theory (DFT) studies that indicated that ethanol oxidation is pH dependent because of its sensitivity to the amount of adsorbed OH [86].

Similar to the ethanol oxidation reaction in acid media, the ethanol oxidation in alkaline media was studied by several techniques including electrochemical methods [87, 88], electrochemistry in combination with FTIR [89, 90], DEMS [91–93], or chromatography [94, 95]. The full oxidation of ethanol to $CO_2$ in alkaline media is associated with the production of 12 electrons for each mole of ethanol; however, the challenge remains to fully oxidize the ethanol to $CO_2$ and not to end up with acetaldehyde or acetic acid, because both diminish the faradaic efficiency of the oxidation reaction [95]. The formation of acetic acid is considered a dead end as it is considered a final product that cannot be further oxidized [57]. On the other hand, acetaldehyde is seen as an active reaction intermediate some of which can be further oxidized once formed on the catalyst surface [87, 88, 95]. It was found that the fuel cell operating temperature is the most important parameter to influence $CO_2$ selectivity [95]. Specifically, increasing the temperature from 60 to 100 °C resulted in an increase in the $CO_2$ current efficiency from 6.0% to 30.6% on a Pd/C anode, in this case.

#### 8.6.4.3 Elevated Temperature Direct Ethanol Fuel Cell Membranes – Pros and Cons

There is some agreement within the DEFC community that in order to accelerate the kinetics of the ethanol oxidation reaction and thus reduce the loading of the precious metal catalysts used, higher operation temperatures are needed [45, 55, 65, 66, 87, 94, 96, 97]. This will require an electrolyte membrane suitable for these temperatures. Mechanical, thermal, and cycle stability as well as high ionic conductivity have to be met by the membrane material. Perfluorosulfonic membranes

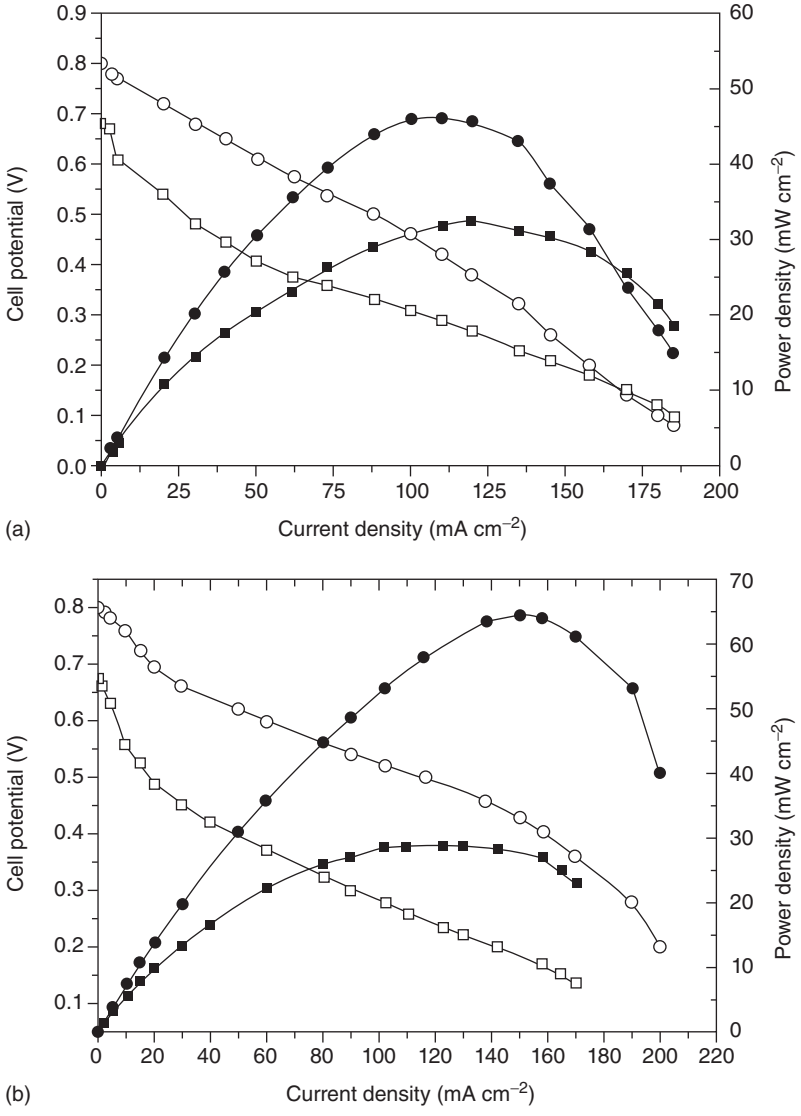


**Figure 8.28** Polarization curves and power density curves in a single DEFC with Pt–Sn/C (2 : 1) and Pt–Ru/C (1 : 1) catalysts. (a) Pt–Sn/C-a (prepared by the deposition of Sn on preformed Pt/C) and commercial Pt–Ru/C, (b) Pt–Sn/C-b (prepared by simultaneous deposition of Pt and Sn on the carbon support) and in-house Pt–Ru/C. Cell temperature: 90 °C. Anode Pt loading: 1.3 mg cm$^{-2}$; ethanol solution: 1.0 M ethanol solution, flow rate: 1.0 ml min$^{-1}$. Cathode: 20 wt% Pt/C, Pt loading 1.0, oxygen pressure: 2 atm Electrolyte: Nafion® 115 membrane. Circles: Pt–Sn/C; squares: Pt–Ru/C. Open symbols: cell potentials; full symbols: power densities. (Reprinted from Ref. [67], Copyright (2005), with permission from Elsevier.)

of the Nafion type are usually considered as first choice for PEMFCs. Nafion membranes are not suitable for a DEFC working at intermediate temperatures because they release water at temperatures higher than 373 K, which results in ionic conductivity deterioration, and the glass transition temperature lies around 403 K [98]. Modifications of Nafion membranes with metal oxides $MO_2$ (M = Zr, Si, Ti) resulted in noticeable improvement in their thermomechanical stability. Nafion-$ZrO_2$ outperforms unmodified Nafion membranes in terms of water uptake and conductivity, but this modification can raise the maximum operation temperature only up to 393 K [99]. Other oxygen ion and proton conductors that do not contain water and can operate in the intermediate temperature range 400–800 K for fuel cell applications are still in a development stage [100].

Proton conductors made either from salts of inorganic oxygen acids [101] or inorganic materials that do not contain water [102] as well as ionic lattice conduction of oxide ceramics suitable for operation at 773 K [103, 104] were intensively investigated. Shimada *et al*. [66] presented a DEFC working in a temperature range of 508–533 K. In this work, $CsH_2PO_4/SiO_2$ ($SiO_2$: 1 wt%) electrolyte was employed to manufacture the MEA. $CsH_2PO_4$ is a hydrogen-bonded oxyacid proton-conducting material that exhibits a reversible phase transition at $T_c = 503$ K [105, 106]. The high temperature cubic phase is stable and shows a high conductivity of $>10^{-2}$ S·cm$^{-1}$ under appropriate humidity conditions [105]. The $SiO_2$ added to the electrolyte enhances the overall conductivity due to its hydrophilicity and the introduction of point defects. However, it was found that the high conductivity of $CsH_2PO_4$ can only be maintained in the relatively narrow temperature range from 508 to 533 K, which requires high pressure or humidity [107]. Ammonium polyphosphate ($NH_4PO_3$) is another possible candidate for a membrane material for intermediate DEFCs [107–110]. Haufe *et al*. [109] studied the polyphosphate composite $[NH_4PO_3]_6[(NH_4)_2SiP_4O_{13}]$ by chemical analysis, X-ray diffraction, thermal gravimetry, impedance spectroscopy, and NMR techniques at temperatures up to 573 K. It was found that the material is stable but after an initial weight loss due to ammonia release and exhibits a high conductivity of 0.1 S·cm$^{-1}$, as can be seen in Figure 8.29. Matsui *et al*. [111, 112] reported high conductivities for the composites $[NH_4PO_3]_6[(NH_4)_2MP_4O_{13}]$ (M = Ti and Si) with activation energies as low as 0.39 and 0.21 eV, respectively, in ambient air. They reported structural changes at intermediate temperatures, which resulted in peculiar ionic-conducting properties and could not assign the observed effect to either the matrix or the decomposed species. This was later clearly answered by Wang *et al*. who investigated a series of six composites with the structure $[NH_4PO_3]_6[(NH_4)_2Si_{1-x}Ti_xP_4O_{13}]$ ($0 \leq x \leq 1$) and concluded that the contribution of the metal cations to the transport properties is minor [113]. Once more, they confirmed high conductivities in a temperature range of 400–550 K. In general, it was shown that the ammonium polyphosphate materials could prove to be a good candidate for intermediate temperature fuel cells as they feature high conductivity in the desired temperature range (423–473 K) [114, 115]. This is associated with small activation energies providing sufficient conductivity down to room temperature. Recently, the preparation of a flexible

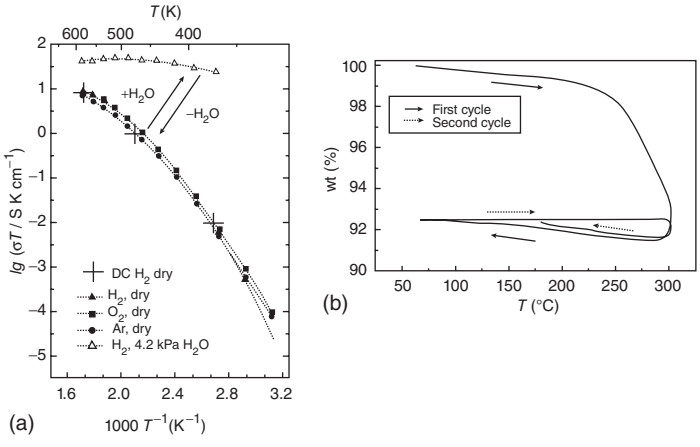


**Figure 8.29** (a) Arrhenius plot of conductivity $\sigma T$ determined in various atmospheres by AC conductivity measurements. Only three values, denoted by +, are determined by DC measurements in a $H_2-H_2$ cell. (b) Mass loss of $[NH_4PO_3]_6[(NH_4)2SiP_4O_{13}]$ at a heating rate of 10 K min$^{-1}$ in a dry $H_2$ atmosphere. (Reprinted from Ref. [109], Copyright (2005), with permission from Elsevier.)

membrane was achieved, making the fabrication of a MEA more straightforward [116]. Future work should be aimed at either improving mechanical stability or at gaining a deeper understanding of the adsorption/desorption process of water, which is correlated with the mechanism of ion transport. A review on the status of alkaline anion-exchange membranes (AAEMs) for alkaline fuel cells [117] or reviews on alkaline fuel cells with a section dedicated to AAEMs [118, 119] were published recently. It is stated that besides considerable efforts, commercial AEMs are in an early stage of development. Key issues are to explain the transport mechanism of hydroxide anions and to increase the conductivity [117]. Another constraint is the precipitation of carbonates from the $CO_2$ generated at the anode on the electrode, which can destroy the active layer [118, 120].

### 8.6.5 Model Catalysts

Significant amount of work was performed in order to investigate the reaction mechanism of the ethanol oxidation reaction on various electrode materials including polycrystalline platinum and platinum-based alloys of other metals such as tin, ruthenium, or rhodium supported on carbon materials. However, designing and tuning the catalysts' activity by careful control of their compositional and structural properties, down to the level of atoms, is one of the ultimate goals of catalysis. This would lay the foundation for an "atomistic engineering" of catalyst surfaces [121]. The activity toward a certain reaction is a measure of how well the catalyst promotes the reaction by enabling the four functions of a catalyst: Firstly, the catalyst adsorbs the target molecule and cleaves some of its bonds.

It then retains the reactants at close proximity to the surface. By definition, the catalyst facilitates the targeted reaction or even enables new pathways. And lastly, when the desired reaction takes place, the catalyst has to release the products so that the catalyst site becomes active again.

As real catalyst systems are rather complex to investigate, it is very beneficial to use an approach where a model catalyst is correlated with the various parameters of catalyst activity. These parameters include the composition of the catalyst nanoparticles, their size [122–124], their dispersion [125, 126], the coordination of surface atoms [127, 128], and the influence of the support material [129–131]. Enhanced mass transport due to spherical diffusion toward 0D particles also has to be considered [132–134].

#### 8.6.5.1 Creating Nanostructured Model Surfaces

Well-defined electrode surfaces are of the greatest importance for the fundamental understanding of reactions at interfaces. Therefore, single crystals and highly oriented pyrolytic graphite (HOPG), show a very high degree of three-dimensional ordering, and are employed as model electrodes or as support for dispersed particles [135–137]. For single crystals, the orientation of the crystal face can influence the kinetics. The second step in creating a model catalyst system, after creating a well-defined surface, is the deposition of single particles or small clusters onto the surface. There are several ways [138, 139] to form nanostructured modifications on surfaces; these include electrochemical deposition or top-down lithography methods. The different methods of how nanolithography can be performed by either a scanning tunneling microscope (STM) or an electrochemical scanning tunneling microscope (EC-STM) were extensively reviewed [140, 141]. A STM tip can be used for the creation of nucleation centers by mechanical interaction between the tip and the substrate [142]. The local removal of a tarnishing film with the tip followed by electrodeposition results in metal deposition only at the freshly uncovered sites of the surface [143]. A conceptually different method that can be used to create controlled nanostructures using an STM tip is the so-called jump-to-contact method [144–146]. In this method, metal ions from the solution are deposited on the tip [147]. Then the tip is brought to a very close proximity of the surface that the jump-to-contact occurs, leading to the formation of a metal bridge between the substrate and the tip. Successive withdrawal of the tip leaves a small metal cluster on the surface. The main advantages of this method are that it can be performed at kilohertz rates, the STM tip can "read" the produced pattern after "writing" it, and that the cluster size can be controlled within a certain range [140]. Electrochemical metal deposition is a fast and convenient way to modify surfaces with foreign metals from solution in a well-defined manner [137]. Although the actual mechanism of the particle growth is still a subject of scientific debate [148, 149], electrodeposition is an important tool to create supported nanoparticles. Pulse electrodeposition is usually used to form a relatively uniform distribution of nanoparticles, for example, Pt or Au on HOPG surfaces [150]. However, with a single pulse deposition, the reaction may run into mass-transport limitation,

especially when high overpotentials are applied. As the depletion zones overlap more for particles with close and many neighbors, they grow slower and therefore single pulses lead to increasing size dispersion [151, 152]. A short (μs–ms), high-overpotential nucleation pulse followed by a low-overpotential growth pulse is usually used to reduce this diffusional coupling effect. The longer (>1 s) second pulse leads to steady growth of metal particles without further nucleation [153]. It has been recently shown that using the double-pulse technique the size of platinum particles on a boron-doped diamond (1 0 0) surface can be tuned between 1 and 15 nm in height and 5 and 50 nm in apparent radius, while keeping the particle density constant [154].

Once a suitable nanostructured model system has been created to experimentally identify parameters that influence reactivity, the second and third steps are to measure the reactivity of the created nanostructures and to combine these findings, often assisted by theoretical calculations and models, to a valid theory. In the following section, we discuss the status of model catalyst research performed for the ethanol oxidation reaction, both in acidic and alkaline media. Specifically, we elaborate on the influence of coordination, composition, substrate, particle size, and dispersion on the electrocatalytic activity. As it is of significance for the ethanol oxidation reaction (EOR), we treat the degree of alloying of bimetallic catalysts as an additional parameter. In addition, we discuss experiments dealing with temperature dependence of some catalysts for the EOR.

#### 8.6.5.2 **Acidic Media**

To study the kinetics of ethanol oxidation on various Pt single crystal surfaces (i.e., Pt of various coordination numbers), the adsorption of CO and evolution of $CO_2$ on Pt(111), Pt(110), and Pt(100) electrode surfaces were monitored with FTIR while applying potential steps in 0.1 or 1 M EtOH solution in a flow cell [155]. The correlation of the FTIR spectra with CV data of the three Pt basal planes (CV data not shown here) revealed the potential dependence of $CO_{ads}$ coverage and capability of the planes to cleave the C–C bond. Pt(111) was not only found to have the lowest intensity of CO adsorption but it also exhibits the lowest activity toward C–C bond splitting. Both the Pt(100) and the Pt(110) basal planes are more active for C–C bond cleavage than Pt(111). Also, when the C–C splitting rate on Pt(111) was compared with polycrystalline and stepped (Pt(355)) platinum, the Pt(111) basal plane showed a lower activity, as indicated by $CO_2$ production [156]. Colmati *et al.* [157] found that ethanol oxidation on Pt(111) produces mostly acetaldehyde as it showed little or no $CO_{ads}$ coverage. The group was also able to detect a difference in activity between Pt(100) and Pt(110), and assigned the higher C–C splitting activity to the Pt(110) electrode, which was attributed to the high activity of the Pt(110) steps toward C–C splitting. The $CO_{ads}$ oxidation requires adsorbed OH species [68, 72, 84], which is not readily supplied when the entire surface is covered with $CO_{ads}$. Therefore, an intermediate C–C cleavage rate, as obtained for the Pt(554) surface, which is simply a combination of Pt(111) and Pt(110) properties, is found to produce optimal catalytic conditions. Figure 8.30 shows the maximum current density and the peak potential versus

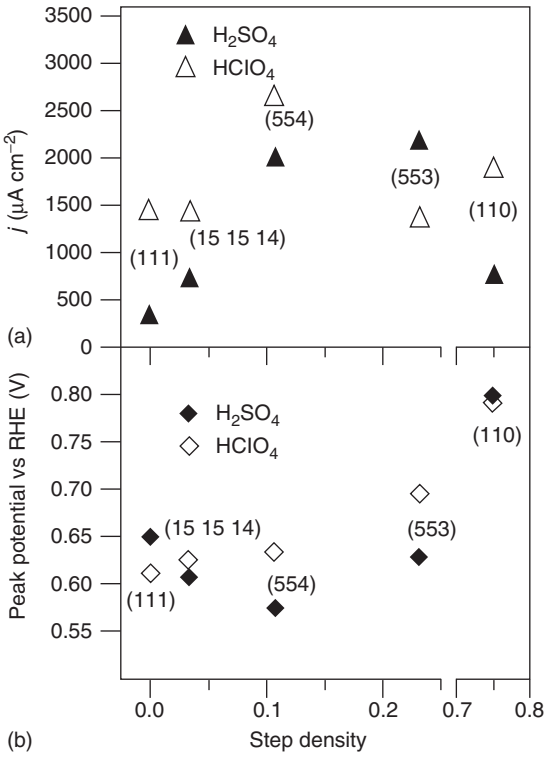


**Figure 8.30** (a) Maximum current density and (b) peak potential versus RHE of bulk ethanol oxidation over step density in 0.5 M $H_2SO_4$ and 0.1 M $HClO_4$ on different Pt model electrodes. (Reprinted with permission from Ref. [158], Copyright (2008), Royal Society of Chemistry.)

reference hydrogen electrode (RHE) of bulk ethanol oxidation on Pt(111), Pt(15 15 14), Pt(554), Pt(553), and Pt(110) electrodes in $H_2SO_4$ and $HClO_4$. The highest current densities were achieved on Pt(554) in $HClO_4$ and on Pt(553) in $H_2SO_4$. The influence of the supporting electrolyte on the electrocatalytic activity can be explained by the preferential adsorption of bi(sulfate) on Pt on terraces rather than on steps [158, 159].

In addition to the coordination of Pt, there is another approach that can be used in order to enhance the electrocatalytic activity, which is changing the composition of the catalyst by combining the Pt with a second metal to obtain a binary catalyst. This can result in a noticeable change in the electronic properties, for example, changes in the adsorption energy, and thus changing the catalytic activity of the Pt (electronic effect). On the other hand, this composition change may allow for a bifunctional mechanism [160]. Some of the metals that are added to Pt in order to enhance its long-term catalytic activity include Ru, Ni, Mo, or Sn [161]. The reasoning behind the bifunctional mechanism is similar to that of the superiority of Pt(554) over Pt(110), although the latter is more active toward C–C

bond cleavage [158, 162]. Pure Pt exhibits the highest activity for the C–C bond cleavage; however, the high coverage of $CO_{ads}$ on platinum results in blocking the Pt sites that are available for $OH_{ads}$, and thus impedes the oxidation of CO to $CO_2$ [62]. The required surface oxygenated species can be supplied by the adjacent cocatalyst atom, allowing for higher catalytic activity [97].

The effect of the addition of a second metal (Ru, Pd, W, and Sn) to Pt was investigated in terms of the platinum lattice parameter [97]. It was found that the addition of Ru or Pd results in decreasing the Pt lattice parameter, while it is increased by alloying Pt with Sn or W. The activity of these binary catalysts for the ethanol oxidation reaction was found to increase in the following order PtPd < PtW < PtRu < PtSn. When various compositions of PtSn catalyst, ranging from $Pt_1Sn_1$ to $Pt_4Sn_1$, were examined for their activities, an almost volcano plot was obtained when the peak power of a DEFC with the respective catalysts over atomic percentage of Sn was plotted.

The apex of the volcano forms due to the interplay between the enhanced activity due to lattice expansion and the decreased conductivity as a result of the higher amounts of semiconducting tin oxide [163]. For temperatures from 60 to 90 °C, the optimal Sn content was found to be 30–40% [97], while a slightly higher value of 50% was found to be the optimum for ethanol oxidation at room temperature [164]. So it was concluded that the operating temperature has an influence on the optimal composition [160]. Increasing the lattice parameter results in changing the Pt electronic properties, and thus the catalytic activity, by shifting the d-band of the Pt down, as reported for $Pt_3Sn$ [165, 166]. It has been reported that the oxidation state of Sn in the bimetallic catalyst, whether it is in the alloy form, such as in Pt–Sn, or in the oxide form, such as in Pt–$SnO_x$, has a pronounced effect on the reaction mechanism [167–169]. Godoi *et al*. investigated the activity of Pt–$SnO_x$ catalysts with different amounts of alloyed and oxidized forms of Sn, while keeping the same overall composition (Pt : Sn = 7 : 3, particle size ≈ 3 nm) [168]. The obtained catalytic activities toward ethanol oxidation were higher for catalysts that were treated in hydrogen atmosphere and therefore showed a higher degree of alloying than for catalysts with a higher amount of oxidized Sn. This enhancement in catalytic activity was attributed to an electronic effect that is caused by increased filling of the Pt 5d band when the degree of alloy increases.

Besides the catalyst itself, the support may play a crucial role in the catalytic activity [134, 170]. Multiwalled carbon nanotubes (MWCNTs) were compared to commercial Vulcan carbon as a support for Pt–Sn catalyst [171]. CO stripping voltammetry and electrochemical impedance spectroscopy results indicate higher exchange currents on the MWCNT support. These higher currents were attributed to the oxygenated surface functional groups on the support that act as nuclei to anchor the Pt–Sn particles, the improved electronic conductivity of the MWCNTs, and the improved metal–support interaction. In a similar manner, Pt and Pt–Ru nanoparticles were investigated on graphene support and compared to graphite and Vulcan substrate [172].

Although well-defined supports, such as HOPG, were employed for studies on the deposition of DEFC-relevant catalysts such as Pt–Sn [173], there are only a

few reports on the influence of model supports on the ethanol oxidation reaction. In a study performed by El-Shafei and Eiswirth [174], Sn sub-monolayers were deposited on Pt(100), Pt(110), and Pt(111) single crystal electrodes and the effect of Sn coverage rate of ethanol oxidation was investigated. For all the three investigated basal planes, the addition of Sn was found to enhance the activity, and the highest increase was reported for Pt(110) on which it led to a more than 10-fold increase in oxidation current. The optimum coverage was found to depend on the basal plane, where 0.2, 0.25, and 0.52 of a monolayer of Sn for Pt(100), Pt(111), and Pt(110), respectively, were reported. Zheng *et al.* [175] performed similar work and it was concluded that Sn adsorbs preferably on the hollow sites of the low-index basal planes Pt(111) and Pt(100); however, it does not show significant adsorption on Pt(110) single crystals.

The influence of particle size was also investigated by comparing the activity of catalysts (Pt/C, Pt–Ru/C, and $Pt_3Sn/C$ ) synthesized via the polyol route with commercial ones [176]; however, no size-induced effects could be observed as a lower degree of alloy formation for the synthesized particles led to a decrease in activity that overlaid other effects (compare [168]). Another study investigated the particle size effects using Pt particles on carbon support in a half-cell. This study revealed a maximum specific activity for a particle size of 2.5 nm. This was attributed to a compromise between structural effects and oxophilicity of the Pt surface [177].

#### 8.6.5.3 Alkaline Media

Although the activity of organic molecule oxidation is higher in alkaline media than in acidic media [178], the ethanol oxidation reaction was much less studied in alkaline media due to some challenges including the carbonation, which leads to membrane deactivation. Lai and Koper [158] investigated the ethanol oxidation reaction in alkaline media on Pt single crystal electrodes. The results indicate that the catalytic activity of ethanol oxidation on all the investigated Pt single crystals in NaOH is significantly higher than in $HClO_4$. The initial current for the ethanol oxidation is higher in alkaline media than in acidic media; however, deactivation of the electrodes is more prominent in the alkaline solution. The deactivation is even stronger for surfaces with wide terraces (Pt(111) and Pt(15 15 14)). This deactivation is due to the formation of adsorbed $CH_x$ species, which cannot be stripped as easily as in acid media [158]. These species were detected in higher amounts on Pt(111) than on Pt(554) surfaces. It was suggested that $CH_{x,ads}$ species are stable only on terrace sites, while they quickly oxidize to $CO_{ads}$ on (110) sites. Also, the onset potential for oxidation currents was found to be as low as 0.35 V versus RHE for Pt(110) in alkaline media [178]. Tian *et al.* [179] used electrodeposited Pd nuclei in order to grow tetra-hexahedral Pd nanocrystals. These nanocrystals predominantly feature [180] facets that are composed of two (210) steps followed by one (310) step. These crystals showed four- to sixfold increase in ethanol oxidation reaction current when compared to commercial Pd-black in 0.1 M EtOH and 0.1 M NaOH. This behavior was attributed to the high concentration of surface atomic steps on these crystals.

For the effect of the catalyst composition on the catalytic activity of ethanol oxidation in alkaline media, it was found that the activity of Pd is slightly higher than that of Pt [92, 181]. However, as for Pt in acidic media, the C–C bond cleavage is rather difficult and acetate ions are the main product [88]. As in acidic media, the addition of Sn to the catalyst was investigated for the ethanol oxidation reaction in alkaline environment [182–184]. Templated Pt–Sn (80 : 20) catalysts showed a slight improvement over templated Pt catalysts [184]. As the observed current densities at lower potentials are higher for the Pt–Sn catalyst, it was hypothesized that the presence of tin oxides facilitates the oxidation of adsorbed intermediates. Antolini and Gonzalez gave an overview about studies investigating the different catalyst systems that were investigated for the ethanol oxidation reaction in alkaline media [118]. In addition to bimetallic $PtM_x$ and $PdM_x$, they list additions of various oxides to Pt/C and Pd/C and also catalyst systems such as Ru–Ni without any Pd or Pt content. Zhu *et al*. [185] reported the observation of a substrate and composition effect when growing Pd on carbon-supported gold nanoparticles. While the absolute ethanol oxidation current is highest for pure Pd on Vulcan carbon, the current per microgram of Pd is highest when measured for a Pd:Au ratio of 1 : 4. This was attributed to a shift in the $Pd_3d$ binding energy, induced by the Au, which weakens the bonding interaction between the adsorbed species and Pd and therefore enhances the anti-poison capabilities of the catalyst [186].

Studies on the influence of the size or dispersion of catalyst nanoparticles on their activity toward ethanol oxidation reaction in alkaline media are rare. One recent publication investigated the activity of spherical Pd nanopoarticles with varying sizes on Ni-foil [187]. To correct for the size-dependent catalyst loading, the measured currents were converted to currents per millimole of Pd and found that nanoparticles with a diameter of 12.0 nm showed a 359 times higher loading-normalized current during CV measurements than catalyst particles with a diameter of 28.8 nm. Particles with intermediate diameters (14.0 and 18.9 nm) followed the same trend. The authors stated that enhancement of intrinsic catalytic activity of the electrodes with smaller particles is due to an increase in "true" surface area and the availability of more energized surface Pd atoms [187].

#### 8.6.5.4 A Few Words about Cathode Catalysts (Conventional and MeOH Tolerant Catalysts)

The ideal material for a DEFC cathode should have a high activity for the ORR and a high tolerance for ethanol oxidation. Pt alloyed with some of the first-row transition metals was found to give a higher activity for ORR than pure platinum in low temperature fuel cells [188–191]. The improvement in the ORR activity obtained when Pt–M alloy electrocatalysts are used was attributed to both geometric (decrease of the Pt–Pt bond distance) [192] and electronic factors (increase of Pt d-electron vacancy) [188]. Ethanol adsorption and oxygen adsorption are competing with each other for the surface sites. Similar to the case of methanol oxidation on Pt surface, the dissociative chemisorption of ethanol requires the existence of ensembles of several adjacent Pt atoms [48, 193], and the presence of foreign atoms around Pt-active sites within these ensembles

could block ethanol adsorption on Pt sites due to the dilution effect. On the other hand, oxygen adsorption requires only two adjacent sites and so it is not affected significantly by the presence of the second metal. In addition to a high ORR activity, Pt–Ni and Pt–Co alloys also presented a good tolerance for methanol oxidation [194–197]. On this basis, many binary alloy electrocatalysts were investigated as an ethanol-tolerant cathode material including Pt–Co and Pt–Pd, both supported on carbon. When a commercially available carbon supported Pt–Co (3 : 1) electrocatalyst was tested in a single DEFC, it was found that in the cathode region of the potential (0.7–0.9 V vs RHE) Pt/C and Pt–Co/C have the same activity for ethanol oxidation [198]. On the other hand, by measurements of oxygen reduction in $H_2SO_4$ in the presence and in the absence of ethanol, promising results were obtained using a Pt–Pd (9 : 1) catalyst [199]. The Pt–Pd/C catalyst possesses about the same ORR activity, but a higher ethanol tolerance than Pt and Pt–Co.

## 8.7
## Conclusions – Folding It Back

In the preceding chapters, a description was given of an autonomous energy system where electrochemical devices play an important role. The problem of energy management is a striking one when various devices for energy conversion and energy storage need to be used. Since technical characteristics of the devices are quite different, a thorough analysis of the primary energy supply is necessarily contrasted by the anticipated electricity demand structure. Here, the importance of a sophisticated procedure as represented by the computer science approach is needed for analysis, control, and optimization of the overall system. Taking this a step further, one can think of implementing computing capabilities into the devices themselves in order to make them "smart," that is, providing intelligence in their operation depending on external factors. So, devices themselves know how their efficiency, time response, expected life time, and so on are under the given parameters such as operating conditions and actual state of health. In the overall context of operation, the devices decide themselves which one takes over a required task in order to fulfill the operational demand. In such a kind of *bottom-up* process hardware components with usually limited technical capabilities but which are continuously operating and being monitored can eventually be improved considerably through software in their functionality in an energy system.

Another aspect, which is almost opposite, is how to improve the hardware itself of components. Achieving a better understanding of the functionality of single components in the complete system allows for a better feedback for a possible hardware optimization of single components. This would be done in a typical *top-down* approach. Having fully understood the main operational parameters of a certain device its improvement can be done in much more focused way.

Combining the various views described in the previous chapters one can see how further developments and improvements in energy systems can be accomplished. In some areas it is a *top-down* approach and in others it is *bottom up.* Understanding the functioning of these different ways in a rather complex system avoids a biased view toward certain ways of solving problems (influenced by the philosophy of a given discipline), be it a scientific or an engineering one. The combination of both, maybe mediated by a discipline such as computer science, can considerably enhance our capabilities to deal with complex systems.

### Acknowledgments

This work was supported in part by TUM CREATE, Singapore. Editing work by Sundar Pethaiah and Jochen Friedl and contributions by David Ciechanowicz are appreciated.

### References

1. Jamshidi, M. (2008) *Systems of Systems Engineering – Principles and Applications*, CRC Publishers, Boca Raton, FL.
2. Geisberger, E. and Broy, M. (eds) (2012) *Agenda CPS, Integrierte Forschungsagenda Cyber-Physical Systems*, Acatech.
3. Hoffman, K. (1972) *Reference Energy Systems and Resource Data for Use in the Assessment of Energy Technologies*.
4. Beller, M. (1980) *Int. J. Energy Res.*, **4**, 235–251.
5. Blesl, M., Schweiker, A., and Schlenzig, C. (1998) *Erweiterung der Analysemöglichkeiten von Net-Work – Der Netzwerkeditor*, Universitaet Stuttgart, Institut fuer Energiewirtschaft und Rationelle Energieanwendung
6. Schaumann, P., Blesl, M., Böhringer, C.F.U., Kühner, R., Läge, E., Molt, S., Schlenzig, C., Stuible, A., and Voß, A. (1998) *Einbindung des ECOLOG-Modells 'E3Net' und Integration neuer methodischer Ansätze in das IKARUS-Instrumentarium (ECOLOG II)*, Universitaet Stuttgart, Institut fuer Energiewirtschaft und Rationelle Energieanwendung
7. Stuible, A. (2002) PlaNet: Ein entscheidungsunterstützendes System für die Energie- und Umweltplanung.
8. Ciechanowicz, D., Aydt, H., Lees, M., Knoll, A., and Hamacher, T. (2013) A Universal Scheme for Modeling Energy Systems.
9. Knoll, A. (2001) *J. Franklin Inst.*, **338**, 669–705.
10. R. Smith, *IEEE Trans. Comput.*, 1980, **C-29**, 1104–1113,.
11. FIPA (2002) Contract Net Interaction Protocol Specification.
12. (2010) EA Energie Architektur GmbH.
13. Agentur für Erneuerbare Energien (2012) Reviews Spezial: Smart Grids, vol. 58.
14. Manara, J. (2007) ZAE Bayern.
15. Dunn, B., Kamath, H., and Tarascon, J. (2011) *Science*, **334**, 928.
16. Linse, C., Huber, C., and Stimming, U. (2013) TUM CREATE, unpublished.
17. Wachtler, M. and Wohlfahrt-Mehrens, M. (2011) ZSW Ulm.
18. Nazri, G.A. and Pastoia, G. (2009) *Lithium Batteries: Science and Technology*, Springer.
19. Etacheri, V., Marom, R., Elazari, R., Salitra, G., and Aurbach, D. (2011) *Energy Environ. Sci.*, **4**, 3243.
20. Zaghib, K., Dontigny, M., Guerfi, A., Charest, P., Rodrigues, I., Mauger,

A., and Julien, C.M. (2011) *J. Power Sources*, **196**, 3949.
21. Albertus, P., Couts, J., Srinivasan, V., and Newman, J. (2008) *J. Power Sources*, **183**, 771.
22. Aurbach, D., Markovsky, B., Amalraj, S.F., Gottlieb, H., Gofer, Y., and Martha, S.K. (2010) *J. Electrochem. Soc.*, **157**, A423.
23. Bruce, P.G., Freunberger, S.A., Hardwick, L.J., and Tarascon, J.M. (2012) *Nat. Mater.*, **11**, 19–30.
24. Lu, Y.C., Gasteiger, H.A., Parent, M.C., Chiloyan, V., and Shao-Horn, Y. (2010) *Electrochem. Solid-State Lett.*, **13**, A69.
25. Ji, X. and Nazar, L.F. (2010) *J. Mater. Chem.*, **20**, 9821–9826.
26. Ji, X., Lee, K.T., and Nazar, L.F. (2009) *Nat. Mater.*, **8**, 500–506.
27. Li, X., Zhang, H., Mai, Z., Zhang, H., and Vankelecom, I. (2011) *Energy Environ. Sci.*, **4**, 1147.
28. Skyllas-Kazacos, M., Chakrabarti, M.H., Hajimolana, S.A., Mjalli, F.S., and Saleem, M. (2011) *J. Electrochem. Soc.*, **158**, R55–R79.
29. Friedl, J., Chen, H.Y., and Stimming, U. (2013) TUM CREATE, unpublished.
30. STROM.info *http://www.strom.info* (accessed July 2013).
31. Kazmerski, L.L. (2013), Homepage of the National Renewable Energy Laboratory (NREL), *http://www.nrel.gov/* (accessed 2013).
32. Laquai, B. (2003) Abschätzung des möglichen Energieertrags einer Photovoltaikanlage, hbw-solar.
33. Larminie, J. and Dicks, A. (2003) *Fuel Cell Systems Explained*, 2nd edn, John Wiley & Sons, Ltd.
34. Turner, J.A. (2004) *Science (Washington)*, **305**, 972–974.
35. Chin, H.-L., Chen, Z.-S., and Chou, C.P. (2003) *Biotechnol. Prog.*, **19**, 383–388.
36. Wang, A., Ren, N., Shi, Y., and Lee, D.-J. (2008) *Int. J. Hydrogen Energy*, **33**, 912–917.
37. Farrauto, R.J. (2003) *Stud. Surf. Sci. Catal.*, **145**, 21–29.
38. Buxbaum, R. and Lei, H. (2003) *J. Power Sources*, **123**, 43–47.
39. Trimm, D.L. and Onsan, Z.I. (2001) *Catal. Rev. Sci. Eng.*, **43**, 31–84.
40. (2002) GM joins Japanese Fuel cell program, abandons methanol. *Fuel Cells Bull.* **2002** (8) 9.
41. Zur, M.D. (2002) *J. Power Sources*, **106**, 35–41.
42. Ren, X., Wilson, M., and Gottesfeld, S. (1996) *J. Electrochem. Soc.*, **143**, 12.
43. Ren, X., Zelenay, P., Thomas, S., Davey, J., and Gottesfeld, S. (2000) *J. Power Sources*, **86**, 11.
44. Thomas, S.C., Ren, X.M., Gottesfeld, S., and Zelenay, P. (2002) *Electrochim. Acta*, **47**, 3741.
45. Lamy, C., Rousseau, S., Belgsir, E.M., Coutanceau, C., and Leger, J.M. (2004) *Electrochim. Acta*, **49**, 3901–3908.
46. EASYCHEM.com.au Advantages and Disadvantages of Ethanol as a Fuel, *http://www.easychem.com.au/production-of-mat'erials/renewable-ethanol/advantages-and-disadvantages-of-ethanol-as-a-fuel* (accessed June 2013).
47. Demirbas, A. (2007) *Prog. Energy Combust. Sci.*, **33**, 1–18.
48. Lamy, C., Lima, A., LeRhun, V., Delime, F., Coutanceau, C., and Leger, J.M. (2002) *J. Power Sources*, **105**, 283–296.
49. Song, S.Q. and Tsiakaras, P. (2006) *Appl. Catal., B*, **63**, 187–193.
50. Zhang, J. and Liu, H. (2009) *Electrocatalysis for Direct Methanol Fuel Cells*, 1st edn, Wiley-VCH Verlag GmbH.
51. Goula, G., Kiousis, V., Nalbandian, L., and Yentekakis, I.V. (2006) *Appl. Catal. Environ.*, **63**, 187.
52. Friedl, J., and Stimming, U. (2013) *Electrochim. Acta*, **101**, 41–58.
53. Hitmi, H., Belgsir, E.M., Leger, J.M., Lamy, C., and Lezna, R.O. (1994) *Electrochim. Acta*, **39**, 407–415.
54. Snell, K.D. and Keenan, A.G. (1982) *Electrochim. Acta*, **27**, 1683–1696.
55. de Souza, J.P.I., Queiroz, S.L., Bergamaski, K., Gonzalez, E.R., and Nart, F.C. (2002) *J. Phys. Chem. B*, **106**, 9825–9830.
56. Fujiwara, N., Friedrich, K.A., and Stimming, U. (1999) *J. Electroanal. Chem.*, **472**, 120–125.
57. Rao, V., Cremers, C., Stimming, U., Cao, L., Sun, S., Yan, S., Sun, G., and Xin, Q. (2007) *J. Electrochem. Soc.*, **154**, B1138–B1147.

58. Wang, H., Jusys, Z., and Behm, R.J. (2004) *J. Phys. Chem. B*, **108**, 19413–19424.
59. Wang, H., Jusys, Z., and Behm, R.J. (2006) *J. Power Sources*, **154**, 351–359.
60. Wang, J., Wasmus, S., and Savinell, R.F. (1995) *J. Electrochem. Soc.*, **142**, 4218–4224.
61. Camara, G.A. and Iwasita, T. (2005) *J. Electroanal. Chem.*, **578**, 315–321.
62. Iwasita, T. and Pastor, E. (1994) *Electrochim. Acta*, **39**, 531–537.
63. Leung, L.W.H., Chang, S.C., and Weaver, M.J. (1989) *J. Electroanal. Chem. Interfacial Electrochem.*, **266**, 317–336.
64. Arico, A.S., Creti, P., Antonucci, P.L., and Antonucci, V. (1998) *Electrochem. Solid-State Lett.*, **1**, 66–68.
65. Rousseau, S., Coutanceau, C., Lamy, C., and Leger, J.M. (2006) *J. Power Sources*, **158**, 18–24.
66. Shimada, I., Oshima, Y., and Otomo, J.-I. (2011) *J. Electrochem. Soc.*, **158**, B369–B375.
67. Song, S.Q., Zhou, W.J., Zhou, Z.H., Jiang, L.H., Sun, G.Q., Xin, Q., Leontidis, V., Kontou, S., and Tsiakaras, P. (2005) *Int. J. Hydrogen Energy*, **30**, 995–1001.
68. Kim, I., Han, O.H., Chae, S.A., Paik, Y., Kwon, S.-H., Lee, K.-S., Sung, Y.-E., and Kim, H. (2011) *Angew. Chem. Int. Ed.*, **50**, 2270–2274, S2270/2271-S2270/2277..
69. Zhao, X., Li, W., Jiang, L., Zhou, W., Xin, Q., Yi, B., and Sun, G. (2004) *Carbon*, **42**, 3251.
70. Li, H., Sun, G., Cao, L., Jiang, L., and Xin, Q. (2007) *Electrochim. Acta*, **52**, 6622–6629.
71. Vigier, F., Coutanceau, C., Hahn, F., Belgsir, E.M., and Lamy, C. (2004) *J. Electroanal. Chem.*, **563**, 81–89.
72. Watanabe, M. and Motoo, S. (1975) *J. Electroanal. Chem. Interfacial Electrochem.*, **60**, 275–283.
73. Markovic, N.M., Gasteiger, H.A., Ross, P.N., Jiang, X.D., Villegas, I., and Weaver, M.J. (1995) *Electrochim. Acta*, **40**, 91–98.
74. Christensen, P.A., Hamnett, A., and Troughton, G.L. (1993) *J. Electroanal. Chem.*, **362**, 207–218.
75. Iwasita, T. (2002) *Electrochim. Acta*, **47**, 3663–3674.
76. Lee, C.G., Umeda, M., and Uchida, I. (2004) 206th Meeting of the Electrochemical Societym Honolulu, HI.
77. Chang, S.C., Leung, L.W.H., and Weaver, M.J. (1990) *J. Phys. Chem.*, **94**, 6013–6021.
78. Spinace, E.V., Neto, A.O., Vasconcelos, T.R.R., and Linardi, M. (2004) *J. Power Sources*, **137**, 17–23.
79. Camara, G.A., de Lima, R.B., and Iwasita, T. (2004) *Electrochem. Commun.*, **6**, 812–815.
80. Kuznetsov, V.I., Belyi, A.S., Yurchenko, E.N., Smolikov, M.D., Protasova, M.T., Zatolokina, E.V., and Duplyakin, V.K. (1986) *J. Catal.*, **99**, 159–170.
81. Radmilovic, V., Richardson, T.J., Chen, S.J., and Ross, P.N. Jr., (2005) *J. Catal.*, **232**, 199–209.
82. Harris, I.R., Norman, M., and Bryant, A.W. (1968) *J. Less Common Met.*, **16**, 427–440.
83. Tripkovic, A.V., Popovic, K.D., Grgur, B.N., Blizanac, B., Ross, P.N., and Markovic, N.M. (2002) *Electrochim. Acta*, **47**, 3707–3714.
84. Morimoto, Y. and Yeager, E.B. (1998) *J. Electroanal. Chem.*, **441**, 77–81.
85. Tripkovic, A.V., Popovic, K.D., and Lovic, J.D. (2001) *Electrochim. Acta*, **46**, 3163–3173.
86. Cui, G., Song, S., Shen, P.K., Kowal, A., and Bianchini, C. (2009) *J. Phys. Chem. C*, **113**, 15639–15642.
87. Fujiwara, N., Siroma, Z., Yamazaki, S.-I., Ioroi, T., Senoh, H., and Yasuda, K. (2008) *J. Power Sources*, **185**, 621–626.
88. Liang, Z.X., Zhao, T.S., Xu, J.B., and Zhu, L.D. (2009) *Electrochim. Acta*, **54**, 2203–2208.
89. Fang, X., Wang, L., Shen, P.K., Cui, G., and Bianchini, C. (2010) *J. Power Sources*, **195**, 1375–1378.
90. Zhou, Z.-Y., Wang, Q., Lin, J.-L., Tian, N., and Sun, S.-G. (2010) *Electrochim. Acta*, **55**, 7995–7999.
91. Bayer, D., Berenger, S., Joos, M., Cremers, C., and Tuebke, J. (2010) *Int. J. Hydrogen Energy*, **35**, 12660–12667.
92. Bayer, D., Cremers, C., Baltruschat, H., and Tuebke, J. (2011) *ECS Trans.*, **41**, 1669–1680.

93. Rao, V., Hariyanto, C., Cremers, C., and Stimming, U. (2007) *Fuel Cells (Weinheim)*, **7**, 417–423.
94. Santasalo-Aarnio, A., Kwon, Y., Ahlberg, E., Kontturi, K., Kallio, T., and Koper, M.T.M. (2011) *Electrochem. Commun.*, **13**, 466–469.
95. Shen, S.Y., Zhao, T.S., and Wu, Q.X. (2012) *Int. J. Hydrogen Energy*, **37**, 575–582.
96. Bianchini, C. and Shen, P.K. (2009) *Chem. Rev. (Washington)*, **109**, 4183–4206.
97. Tsiakaras, P.E. (2007) *J. Power Sources*, **171**, 107–112.
98. Norby, T. (1999) *Solid State Ionics*, **125**, 1–11.
99. Jalani, N.H., Dunn, K., and Datta, R. (2005) *Electrochim. Acta*, **51**, 553–560.
100. Zhu, B., Albinsson, I., Mellander, B.-E., and Meng, G. (1999) *Solid State Ionics*, **125**, 439–446.
101. Zhu, B. (1999) *Solid State Ionics*, **125**, 397–405.
102. Baranov, A.I., Duda, V.M., Jones, D.J., Roziere, J., Sinitsyn, V.V., and Slade, R.C.T. (2001) *Solid State Ionics*, **145**, 241–247.
103. Steele, B.C.H. (2000) *Solid State Ionics*, **129**, 95–110.
104. Zhang, T.S., Chan, S.H., Kong, L.B., Sheng, P.T., and Ma, J. (2009) *Electrochim. Acta*, **54**, 927–934.
105. Otomo, J., Minagawa, N., Wen, C.-J., Eguchi, K., and Takahashi, H. (2003) *Solid State Ionics*, **156**, 357–369.
106. Otomo, J., Nishida, S., Takahashi, H., and Nagamoto, H. (2008) *J. Electroanal. Chem.*, **615**, 84–90.
107. Jiang, Y., Matthieu, T., Lan, R., Xu, X., Cowin, P.I., and Tao, S. (2011) *Solid State Ionics*, **192**, 108–112.
108. Cappadonia, M., Niemzig, O., and Stimming, U. (1999) *Solid State Ionics*, **125**, 333–337.
109. Haufe, S., Prochnow, D., Schneider, D., Geier, O., Freude, D., and Stimming, U. (2005) *Solid State Ionics*, **176**, 955–963.
110. Kenjo, T. and Ogawa, Y. (1995) *Solid State Ionics*, **76**, 29–34.
111. Matsui, T., Takeshita, S., Iriyama, Y., Abe, T., Inaba, M., and Ogumi, Z. (2004) *Electrochem. Commun.*, **6**, 180–182.
112. Matsui, T., Takeshita, S., Iriyama, Y., Abe, T., and Ogumi, Z. (2007) *Solid State Ionics*, **178**, 859–863.
113. Wang, H., Tealdi, C., Stimming, U., Huang, K., and Chen, L. (2009) *Electrochim. Acta*, **54**, 5257–5261.
114. Liu, L., Tu, H., Cremers, C., and Stimming, U. (2006) *Solid State Ionics*, **177**, 2417–2419.
115. Sun, C. and Stimming, U. (2008) *Electrochim. Acta*, **53**, 6417–6422.
116. Kluy, N., Reeb, B.B.L., Paschos, O., Maglia, F., Schneider, O., and Stimming, U. (2012) Proceedings of the 222nd Meeting of the Electrochemical Society, Honolulu, HI.
117. Merle, G., Wessling, M., and Nijmeijer, K. (2011) *J. Membr. Sci.*, **377**, 1–35.
118. Antolini, E. and Gonzalez, E.R. (2010) *J. Power Sources*, **195**, 3431–3450.
119. Zhao, T.S., Li, Y.S., and Shen, S.Y. (2010) *Front. Energy Power Eng. Chin.*, **4**, 443.
120. Varcoe, J.R. and Slade, R.C.T. (2005) *Fuel Cells (Weinheim)*, **5**, 187–200.
121. Hammer, B. and Noerskov, J.K. (1995) *Surf. Sci.*, **343**, 211–220.
122. Friedrich, K.A., Henglein, F., Stimming, U., and Unkauf, W. (2000) *Electrochim. Acta*, **45**, 3283–3293.
123. Maillard, F., Eikerling, M., Cherstiouk, O.V., Schreier, S., Savinova, E., and Stimming, U. (2004) *Faraday Discuss.*, **125**, 357–377; discussion 391–407.
124. Maillard, F., Savinova, E.R., and Stimming, U. (2007) *J. Electroanal. Chem.*, **599**, 221–232.
125. Gasteiger, H.A., Panels, J.E., and Yan, S.G. (2004) *J. Power Sources*, **127**, 162–171.
126. Neyerlin, K.C., Gu, W., Jorne, J., and Gasteiger, H.A. (2007) *J. Electrochem. Soc.*, **154**, B631–B635.
127. Hernandez, F. and Baltruschat, H. (2006) *J. Solid State Electrochem.*, **11**, 877–885.
128. Hernandez, F. and Baltruschat, H. (2006) *Langmuir*, **22**, 4877–4884.
129. Kibler, L.A., El-Aziz, A.M., Hoyer, R., and Kolb, D.M. (2005) *Angew. Chem. Int. Ed.*, **44**, 2080–2084.
130. Roudgar, A. and Gross, A. (2003) *J. Electroanal. Chem.*, **548**, 121–130.

131. Zhou, Y., Pasquarelli, R., Holme, T., Berry, J., Ginley, D., and O'Hayre, R. (2009) *J. Mater. Chem.*, **19**, 7830–7838.
132. Chen, S. and Kucernak, A. (2004) *J. Phys. Chem. B*, **108**, 3262–3276.
133. Quaino, P.M., Fernandez, J.L., Gennero, D.C.M.R., and Chialvo, A.C. (2006) *J. Mol. Catal. A: Chem.*, **252**, 156–162.
134. Wolfschmidt, H., Weingarth, D., and Stimming, U. (2010) *ChemPhysChem*, **11**, 1533–1541.
135. Barber, J., Morin, S., and Conway, B.E. (1998) *J. Electroanal. Chem.*, **446**, 125–138.
136. Gloaguen, F., Leger, J.M., Lamy, C., Marmann, A., Stimming, U., and Vogel, R. (1999) *Electrochim. Acta*, **44**, 1805–1816.
137. Brülle, T. and Stimming, U. (2009) *J. Electroanal. Chem.*, **636**, 10–17.
138. Hiramatsu, M. and Hori, M. (2010) *Materials*, **3**, 1559–1572.
139. Eibeck, P., Spatz, J.P., Möβmer, S., Möller, M., Herzog, T., and Ziemann, P. (1999) *Nanostruct. Mater.*, **12**, 383–386.
140. Kolb, D.M. and Simeone, F.C. (2005) *Electrochim. Acta*, **50**, 2989–2996.
141. Kolb, D.M. and Simeone, F.C. (2006) *Curr. Opin. Solid State Mater. Sci.*, **9**, 91–97.
142. Nyffenegger, R.M. and Penner, R.M. (1997) *Chem. Rev. (Washington)*, **97**, 1195–1230.
143. Petri, M. and Kolb, D.M. (2002) *Phys. Chem. Chem. Phys.*, **4**, 1211–1216.
144. Del, P.M.G., Leiva, E.P.M., Kleine, H., Meier, J., Stimming, U., Mariscal, M., and Schmickler, W. (2003) *Electrochim. Acta*, **48**, 1287–1294.
145. Engelmann, G.E., Ziegler, J.C., and Kolb, D.M. (1998) *Surf. Sci.*, **401**, L420–L424.
146. Kolb, D.M., Ullmann, R., and Will, T. (1997) *Science (Washington)*, **275**, 1097–1099.
147. Kolb, D.M. (2001) *Angew. Chem. Int. Ed.*, **40**, 1162–1181.
148. Hyde, M.E. and Compton, R.G. (2003) *J. Electroanal. Chem.*, **549**, 1–12.
149. Ustarroz, J., Ke, X., Hubin, A., Bals, S., and Terryn, H. (2012) *J. Phys. Chem. C*, **116**, 2322–2329.
150. Zoval, J.V., Lee, J., Gorer, S., and Penner, R.M. (1998) *J. Phys. Chem. B*, **102**, 1166–1175.
151. Fransaer, J.L. and Penner, R.M. (1999) *J. Phys. Chem. B*, **103**, 7643–7653.
152. Penner, R.M. (2001) *J. Phys. Chem. B*, **105**, 8672–8678.
153. Ueda, M., Dietz, H., Anders, A., Kneppe, H., Meixner, A., and Plieth, W. (2002) *Electrochim. Acta*, **48**, 377–386.
154. Brulle, T., Denisenko, A., Sternschulte, H., and Stimming, U. (2011) *Phys. Chem. Chem. Phys.*, **13**, 12883–12891.
155. Xia, X.H., Liess, H.D., and Iwasita, T. (1997) *J. Electroanal. Chem.*, **437**, 233–240.
156. Shin, J., Tornquist, W.J., Korzeniewski, C., and Hoaglund, C.S. (1996) *Surf. Sci.*, **364**, 122–130.
157. Colmati, F., Tremiliosi-Filho, G., Gonzalez, E.R., Berna, A., Herrero, E., and Feliu, J.M. (2009) *Faraday Discuss.*, **140**, 379–397.
158. Lai, S.C.S. and Koper, M.T.M. (2009) *Phys. Chem. Chem. Phys.*, **11**, 10446–10456.
159. Mostany, J., Herrero, E., Feliu, J.M., and Lipkowski, J. (2002) *J. Phys. Chem. B*, **106**, 12787–12796.
160. Antolini, E. and Gonzalez, E.R. (2011) *Catal. Today*, **160**, 28–38.
161. Zignani, S.C., Gonzalez, E.R., Baglio, V., Siracusano, S., and Arico, A.S. (2012) *Int. J. Electrochem. Sci.*, **7**, 3155–3166.
162. Colmati, F., Tremiliosi-Filho, G., Gonzalez, E.R., Berna, A., Herrero, E., and Feliu, J.M. (2009) *Phys. Chem. Chem. Phys.*, **11**, 9114–9123.
163. Zhou, W.J., Song, S.Q., Li, W.Z., Zhou, Z.H., Sun, G.Q., Xin, Q., Douvartzides, S., and Tsiakaras, P. (2005) *J. Power Sources*, **140**, 50–58.
164. Kim, J.H., Choi, S.M., Nam, S.H., Seo, M.H., Choi, S.H., and Kim, W.B. (2008) *Appl. Catal., B*, **82**, 89–102.
165. Garcia-Rodriguez, S., Somodi, F., Borbath, I., Margitfalvi, J.L., Pena, M.A., Fierro, J.L.G., and Rojas, S. (2009) *Appl. Catal., B*, **91**, 83–91.
166. Liu, P., Logadottir, A., and Norskov, J.K. (2003) *Electrochim. Acta*, **48**, 3731–3742.

**167.** Colmati, F., Antolini, E., and Gonalez, E.R. (2007) *J. Electrochem. Soc.*, **154**, B39–B47.

**168.** Godoi, D.R.M., Perez, J., and Villullas, H.M. (2010) *J. Power Sources*, **195**, 3394–3401.

**169.** Jiang, L., Colmenares, L., Jusys, Z., Sun, G.Q., and Behm, R.J. (2007) *Electrochim. Acta*, **53**, 377–389.

**170.** Eikerling, M., Meier, J., and Stimming, U. (2003) *Z. Phys. Chem. (Muenchen)*, **217**, 395–414.

**171.** Thomas, J.E., Bonesi, A.R., Moreno, M.S., Visintin, A., Castro, L.A.M., and Triaca, W.E. (2010) *Int. J. Hydrogen Energy*, **35**, 11681–11686.

**172.** Dong, L., Gari, R.R.S., Li, Z., Craig, M.M., and Hou, S. (2010) *Carbon*, **48**, 781–787.

**173.** Yao, Y., Fu, Q., Zhang, Z., Zhang, H., Ma, T., Tan, D., and Bao, X. (2008) *Appl. Surf. Sci.*, **254**, 3808–3812.

**174.** El-Shafei, A.A. and Eiswirth, M. (2010) *Surf. Sci.*, **604**, 862–867.

**175.** Zheng, Q.-W., Fan, C.-J., Zhen, C.-H., Zhou, Z.-Y., and Sun, S.-G. (2008) *Electrochim. Acta*, **53**, 6081–6088.

**176.** Colmenares, L., Wang, H., Jusys, Z., Jiang, L., Yan, S., Sun, G.Q., and Behm, R.J. (2006) *Electrochim. Acta*, **52**, 221–233.

**177.** Perez, J., Paganin, V.A., and Antolini, E. (2011) *J. Electroanal. Chem.*, **654**, 108–115.

**178.** Spendelow, J.S. and Wieckowski, A. (2007) *Phys. Chem. Chem. Phys.*, **9**, 2654–2675.

**179.** Tian, N., Zhou, Z.-Y., Yu, N.-F., Wang, L.-Y., and Sun, S.-G. (2010) *J. Am. Chem. Soc.*, **132**, 7580–7581.

**180.** Antolini, E. (2007) *J. Power Sources*, **170**, 1–12.

**181.** Xu, C., Cheng, L., Shen, P., and Liu, Y. (2007) *Electrochem. Commun.*, **9**, 997–1001.

**182.** He, Q., Chen, W., Mukerjee, S., Chen, S., and Laufek, F. (2009) *J. Power Sources*, **187**, 298–304.

**183.** Jiang, L., Hsu, A., Chu, D., and Chen, R. (2010) *Int. J. Hydrogen Energy*, **35**, 365–372.

**184.** Switzer, E.E., Olson, T.S., Datye, A.K., Atanassov, P., Hibbs, M.R., and Cornelius, C.J. (2009) *Electrochim. Acta*, **54**, 989–995.

**185.** Zhu, L.D., Zhao, T.S., Xu, J.B., and Liang, Z.X. (2009) *J. Power Sources*, **187**, 80–84.

**186.** Enache, D.I., Edwards, J.K., Landon, P., Solsona-Espriu, B., Carley, A.F., Herzing, A.A., Watanabe, M., Kiely, C.J., Knight, D.W., and Hutchings, G.J. (2006) *Science (Washington)*, **311**, 362–365.

**187.** Roy, P.S., Bagchi, J., and Bhattacharya, S.K. (2012) *Catal. Sci. Technol.*, **2**, 2302–2310.

**188.** Antolini, E., Passos, R.R., and Ticianelli, E.A. (2002) *Electrochim. Acta*, **48**, 263–270.

**189.** Mukerjee, S., Srinivasan, S., Soriaga, M.P., and McBreen, J. (1995) *J. Electrochem. Soc.*, **142**, 1409–1422.

**190.** Norskov, J.K., Rossmeisl, J., Logadottir, A., Lindqvist, L., Kitchin, J.R., Bligaard, T., and Jonsson, H. (2004) *J. Phys. Chem. B*, **108**, 17886–17892.

**191.** Toda, T., Igarashi, H., Uchida, H., and Watanabe, M. (1999) *J. Electrochem. Soc.*, **146**, 3750–3756.

**192.** Jalan, V. and Taylor, E.J. (1983) *J. Electrochem. Soc.*, **130**, 2299–2301.

**193.** Gasteiger, H.A., Markovic, N., Ross, P.N., and Cairns, E.J. (1994) *Electrochim. Acta*, **39**, 1825–1832.

**194.** Antolini, E., Salgado, J.R.C., and Gonzalez, E.R. (2005) *J. Electroanal. Chem.*, **580**, 145–154.

**195.** Antolini, E., Salgado, J.R.C., and Gonzalez, E.R. (2006) *J. Power Sources*, **155**, 161–166.

**196.** Salgado, J.R.C., Antolini, E., and Gonzalez, E.R. (2005) *Appl. Catal., B*, **57**, 283–290.

**197.** Yang, H., Coutanceau, C., Leger, J.M., Alonso-Vante, N., and Lamy, C. (2005) *J. Electroanal. Chem.*, **576**, 305–313.

**198.** Lopes, T., Antolini, E., Colmati, F., and Gonzalez, E.R. (2007) *J. Power Sources*, **164**, 111–114.

**199.** Lopes, T., Antolini, E., and Gonzalez, E.R. (2008) *Int. J. Hydrogen Energy*, **33**, 5563–5570.